Scientific Reports

https://doi.org/10.1038/s41598-026-41856-x

Article in Press

Qualitative analysis of chemical components in Berberis kaschgarica Rupr. and study on the in vitro anti-inflammatory effects of its alkaloids

Received: 6 September 2025

Accepted: 23 February 2026

Published online: 02 March 2026

Cite this article as: Ainiwaer S., Dilimulati D., Wumaier A. *et al.* Qualitative analysis of chemical components in Berberis kaschgarica Rupr. and study on the in vitro anti-inflammatory effects of its alkaloids. *Sci Rep* (2026). https://doi.org/10.1038/s41598-026-41856-x

Saimire Ainiwaer, Dilihuma Dilimulati, Ainiwaer Wumaier & Wenting Zhou

Article

Qualitative Analysis of Chemical Components in Berberis kaschgarica Rupr. and Study on the In Vitro Anti-Inflammatory Effects of its Alkaloids

Saimire Ainiwaer [1,2,3,4,†], Dilihuma Dilimulati[1,2,3,4,†], Ainiwaer Wumaier [1,2,3,4*],Wenting Zhou [1,2,3,4*]

[1] Department of Pharmacology, School of Pharmacy, Xinjiang Medical University, Urumqi, Xinjiang P.R. China. samiraanwar@163.com (S.A.); dilihuma@stu.xjmu.edu.cn (D.D.)
[2] Xinjiang Key Laboratory of Active Components and Drug Release Technology of Natural Medicines, Urumqi 830017, Xinjiang, China.
[3] Xinjiang Key Laboratory of Biopharmaceuticals and Medical Devices, Urumqi 830017, China
[4] Engineering Research Center of Xinjiang and Central Asian Medicine Resources, Ministry of Education, Urumqi 830017, China
[*] Ainiwaer Wumaier: 2249816583@qq.com; Wenting Zhou: zwt@xjmu.edu.cn;
[†] These authors contributed equally to this work.

Abstract

Background: *Berberis kaschgarica Rupr.* fruits (BKF) can reduce blood pressure, regulate blood lipid levels, and exert anti-inflammatory and anti-oxidative effects. Additionally, alkaloids are among the active components in BKF. **Methods:** Sensitive and selective high-performance liquid chromatography with mass spectrometry, network pharmacology, and bioinformatic analysis was conducted. **Results:** We identified 544 metabolites and 105 secondary metabolites from BFK. Among the secondary metabolites, 24 were alkaloids. Moreover, there were 583 potential drug targets and 4,481 human anti-atherosclerosis targets. Finally, 366 intersecting targets of BFK against atherosclerosis were identified. These targets were enriched in 546 terms in biological processes, 48 terms in cell components, 121 terms in molecular functions, and 36 signaling pathways. Notably, 18 of the 24 alkaloids were fat-soluble alkaloids (FSA), and the remaining 6 were water-soluble alkaloids (WSA). Because oxyberberine (OBB) was predicted to have an ideal anti-atherosclerosis effect and was further studied. We established four intervention groups: FSA, WSA, total alkaloids (TA), and OBB. The effects of these alkaloids on caspase-11-induced pyroptosis and TLR4-induced inflammation in LPS-stimulated mouse macrophages in vitro were explored. The anti-pyroptosis results demonstrated significant evaluation in caspase-11, caspase-1, IL-1β, IL-18, and, GSDMD. Additionally, there were significant decreases in MMP3 and MMP9 in the supernatant, as well as the expression of TLR4 and pSTAT3. **Conclusions:** Conclusively, BKF contains numerous effective components, making it a valuable natural medicinal material with substantial developmental and utilitarian potential. In in vitro experiments, the alkaloids from BKF can reduce the LPS-induced expression of caspase-11 and GSDMD. Compared with previous studies on BKF, which had gaps in systematic identification of bioactive subtypes via basic colorimetry and unclear anti-AS mechanisms. our study advances research by using UPLC-MS/MS for the first time to identify 544 metabolitesin BKF, establishing a comprehensive metabolite profile and integrating network pharmacology and in vitro assays to first link BKF alkaloids to regulating

caspase-11-mediated pyroptosis and TLR4-induced inflammation. Moreover, our findings contribute to compositional innovation, mechanistic breakthroughs, and translational value.

Keywords: *Berberis Kaschgarica Rupr.*; Alkaloids; Inflammation; Pyroptosis.

1. Introduction

In China, Berberis spp. is commonly referred to as "Sankezhen" and "Xiaohuanglian" [1,2]. Berberis Kaschgarica Rupr. serves as a significant constituent of the Berberidaceae family in western China. Berberis Kaschgarica Rupr. fruit (BKF) is widely used as a traditional medicine for treating hyperlipidemia and hypertension by residents. BKF contains various phytochemicals, including flavonoids, coumarins, saccharides, glycosides, saponins, amino acids, proteins, organic acids, volatile oils, and more [3-5] Anthocyanins and polyphenols in BKF exhibit potent antioxidant and free radical scavenging properties [6]. The aqueous extracts of BKF have mass concentration-dependent relaxation effects on the pre-contracted vascular ring [7]. Nonetheless, the precise active components for the beneficial effects of Berberis Kaschgarica Rupr. remain unknown.

Macrophages are pivotal in the onset and progression of atherosclerosis (AS), from its onset to the expansion of the lesion [8]. These cells are the primary contributors to AS plaques, coordinating various biological functions ranging from endothelial damage to AS plaque rupture [9]. The M1 type, also known as the classical inflammatory phenotype of macrophages, can be induced in vitro by lipopolysaccharide (LPS). M1 macrophages primarily contribute to the progression of AS [10]. Macrophage death, when it occurs, can lead to the expansion of the necrotic core and instability of the plaque. Recently, it has been suggested that different programmed deaths, including apoptosis, pyroptosis, and ferroptosis, can occur in plaque-residing macrophages [11]. Targeted pharmacotherapy of these mechanisms holds promise in maintaining the stability of vulnerable plaques.

Pyroptosis, an inflammatory mode of cell demise, is pivotal in fueling the inflammatory process. While it can protect host cells from microbial pathogens, its dysregulation is closely associated with various autoimmune and inflammatory diseases [12,13]. Consequently, pyroptosis, a form of programmed cell death associated with inflammation, has become a new research hotspot in the field of atherosclerosis (AS) [14 - 16]. The activation of interleukin - 1β (IL - 1β) and interleukin - 18 (IL - 18) is known to fuel the advancement of AS [9]. Furthermore, pyroptosis is initiated by the cleaved form of Gasdermin D.

Toll - like receptor 4 (TLR4), which serves as the primary receptor for lipopolysaccharide (LPS), participates in LPS - mediated cell activation and damage. The Janus kinase - signal transducer and activator of transcription 3 (JAK - STAT3) pathway is implicated in the onset and advancement of atherosclerosis (AS) [17,18]. STAT proteins, especially STAT3, act as crucial transcription factors in the regulation of LPS - triggered inflammatory responses, especially in the secretion of pro - inflammatory cytokines by macrophages [19].

Matrix metalloproteinases (MMPs) are thought to facilitate the transition of stable atherosclerotic lesions to unstable ones. Among them, MMP3 and MMP9, two members of the MMP family, are strongly linked to the stability of AS plaques. MMP3, also called matrix degradation factor 1, is secreted by multiple cell types, including macrophages [20]. It can activate MMP9. Clinical studies have found a positive correlation between MMP3 levels and the incidence of cardiovascular and cerebrovascular events. MMP9, or gelatinase B, is mainly produced by activated macrophages and vascular smooth muscle cells. In AS models, the absence of MMP9 leads to a decrease in aortic burden, a reduction

in the infiltration of damaged macrophages, and less collagen deposition [21]. Moreover, there is a positive association between MMP9 and the vulnerability of atherosclerotic plaques [22].

Under normal physiological conditions, tissue inhibitors of metalloproteinases (TIMPs) precisely control MMP activation, maintaining the dynamic equilibrium of the extracellular matrix [23].

In this study, a qualitative analysis of the chemical components of BKF was performed using the UPLC-MS/MS analysis method. Afterward, a network pharmacology approach was used to identify the potential targets of 24 selected alkaloids and their interaction with AS. This allowed for the preliminary prediction of the medicinal value of alkaloids in *Berberis kaschgarica Rupr.* (ABK) concerning AS. Based on the in vitro RAW264.7 macrophage model and network pharmacology predictions, the alkaloids from BKF particularly oxyberberine (OBB) and fat-soluble alkaloids (FSA) demonstrate preliminary potential in counteracting atherosclerosis (AS)-related pathological processes. However, their in vivo anti-AS efficacy requires further validation using models such as ApoE$^{-/-}$ mice. Our findings may provide some theoretical and experimental basis for the further development of the medicinal value of BKF and the later research on its prevention and treatment of AS.

2. Results

The main goals of the study were to analysis the chemical components in *berberis kaschgarica* Rupr. and discover the anti-inflammatory effects of its alkaloids in vitro. In Figure 1, the study's flowchart is displayed. In this paper, secondary metabolites of BKF were identified using ultra-performance liquid chromatography-tandem mass spectrometry (UPLC-MS/MS). The total ion current (TIC) chromatograms reflect the separation of metabolites. Targets associated with atherosclerosis were retrieved via GeneCardsSuite, and the overlapping targets (Venn diagram) of the disease and BKF metabolites were screened. A protein-protein interaction (PPI) network was constructed to visualize the interaction relationships among core targets while KEGG and GO enrichment analyses clarify the potential biological functions and signaling pathways of the targets. The anti-inflammatory activity of alkaloids from BKF was evaluated in LPS-stimulated RAW264.7 cells: graphs show the regulatory effects of ABK/OBB on cell pyroptosis-related indicators; Western blot demonstrate the inhibitory effects of ABK/OBB on TLR4-mediated inflammatory responses, verifying the in vitro anti-inflammatory potential of the metabolites.

2.1.Qualitative analysis of secondary metabolites in BKF

To systematically characterize the chemical composition of Berberis kaschgarica Rupr. fruits (BKF), ultra-performance liquid chromatography-tandem mass spectrometry (UPLC-MS/MS) was employed. All mass spectrometry (MS) data were processed using Analyst 1.6.3 software to ensure data accuracy and reproducibility.

The UPLC separation was performed on a Shim-pack UPLC SHIMADZU CBM30A column, with a mobile phase consisting of Solvent A (ultrapure water containing 0.04% acetic acid) and Solvent B (acetonitrile containing 0.04% acetic acid) under a gradient elution program: initial conditions (95% A, 5% B) maintained for 0 min, linear gradient to 5% A/95% B over 10 min, hold for 1 min, then rapid reversion to 95% A/5% B within 0.10 min and equilibration for 2.9 min. The column oven temperature was set at 40°C, and the injection volume was 2 μL.

For MS detection, an API 6500 Q TRAP UPLC/MS/MS system with an ESI Turbo Ion-Spray interface was operated in dual polarity mode (positive and negative ionization). The instrument was calibrated using 10 μmol/L polypropylene glycol (for QQQ mode) and 100 μmol/L polypropylene glycol (for linear ion trap mode) to ensure precise mass measurement. Nitrogen was used as the collision gas (5 psi) for multiple reaction monitoring (MRM), and MRM transitions for each metabolite were optimized by adjusting declustering potential and collision energy to enhance detection specificity.

To verify data reliability, mixed quality control (mixed QC) samples—prepared by pooling equal aliquots of all BKF test samples—were analyzed intermittently (once every 8 test samples). The total ion current (TIC) chromatograms of mixed QC samples (Figure 2) showed high overlap in both positive and negative ionization modes, with retention time deviations ≤ 0.1 min and relative standard deviation (RSD) of major peak areas < 30%. This results showed that the TIC curves of metabolite detection exhibited high overlap, with consistent retention times and peak intensities. This indicates that the mass spectrometer had good signal stability when detecting the same sample at different times. The high stability of the instrument provides an important guarantee for the reproducibility and reliability of the data.And the multi-peak chromatogram of metabolite detection by MRM is illustrated in Figure 3. This confirmed the stability of the UPLC-MS/MS system and the credibility of metabolite detection data.

Through the above detection, a total of 544 metabolites were detected in BKF, among which 105 were confirmed as secondary metabolites (Table 1) with identification accuracy > 95%. These secondary metabolites were classified into 8 major classes based on their chemical structures and biosynthetic pathways, covering acids, alkaloids, saccharides, flavonoids, lignans, coumarins, tannins and phenols. Figure 4 shows the 2D structures of components identified in BKF. The 2D chemical structures of 105 secondary metabolites identified from BKF, including alkaloids, flavonoids, phenols, and other categories. The structural diversity of these compounds reflects the richness of the secondary metabolite profile of BKF, and this diversity is a key premise for BKF to potentially exert multi-target and multi-pathway regulatory effects.

Notably, alkaloids (24 compounds) were prioritized as the core research focus for subsequent experiments, as they are well-documented as the major bioactive components of Berberis spp. with anti-inflammatory, lipid-regulating, and anti-atherosclerotic potential [3,6,8]—aligning with the study's objective of exploring BKF's role in atherosclerosis prevention. Among these 24 alkaloids, 18 were classified as fat-soluble alkaloids (FSA, LogP > 1.0) and 6 as water-soluble alkaloids (WSA, LogP < 1.0) based on their lipophilic partition coefficients (LogP values) and literature reports, facilitating targeted functional validation in later in vitro assays.

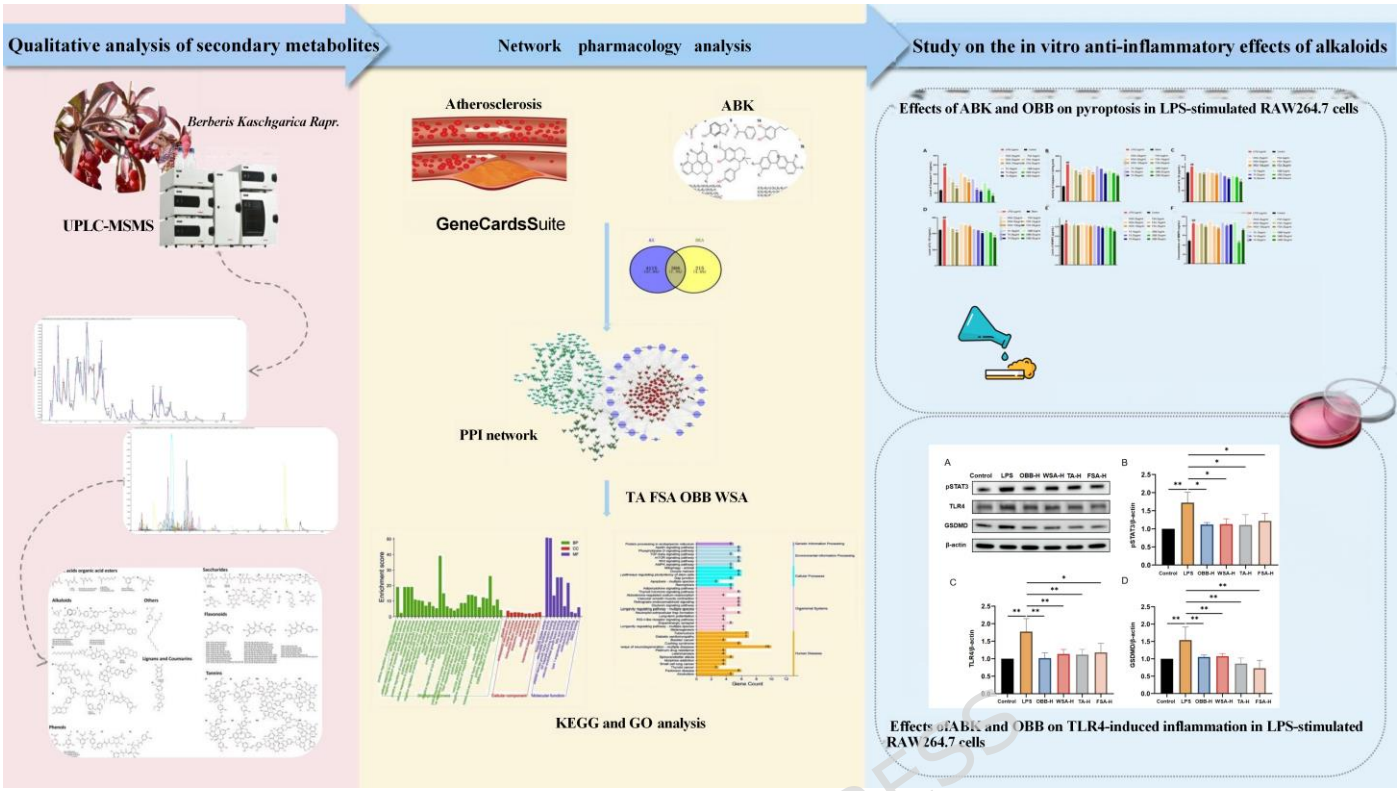

Figure. 1 Research Flowchart for this study.

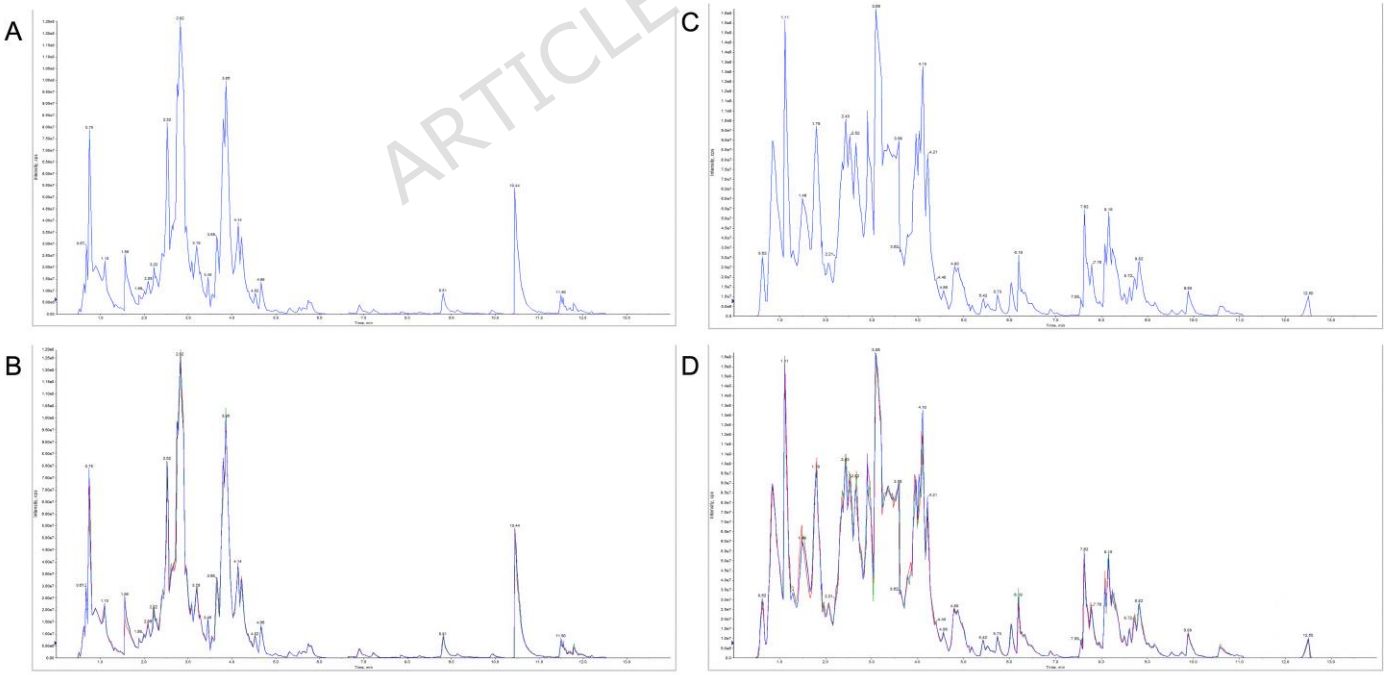

Figure. 2 Total ion current Chromatogram (TIC) of mass spectrometric analysis of the mixed sample. (A) The TIC in Negative Ion Mode for mixed sample; (B) TIC overlay of mixed QC samples detected in Negative Ion Mode; (C) The TIC in Positive Ion Mode for mixed sample; (D) TIC overlay of mixed QC samples detected in Positive Ion Mode. Mixed QC samples were prepared by mixing equal aliquots of all experimental samples to cover the major analytes in the test samples. A total of 10 mixed QC samples were injected intermittently to monitor the stability of the mass spectrometer.

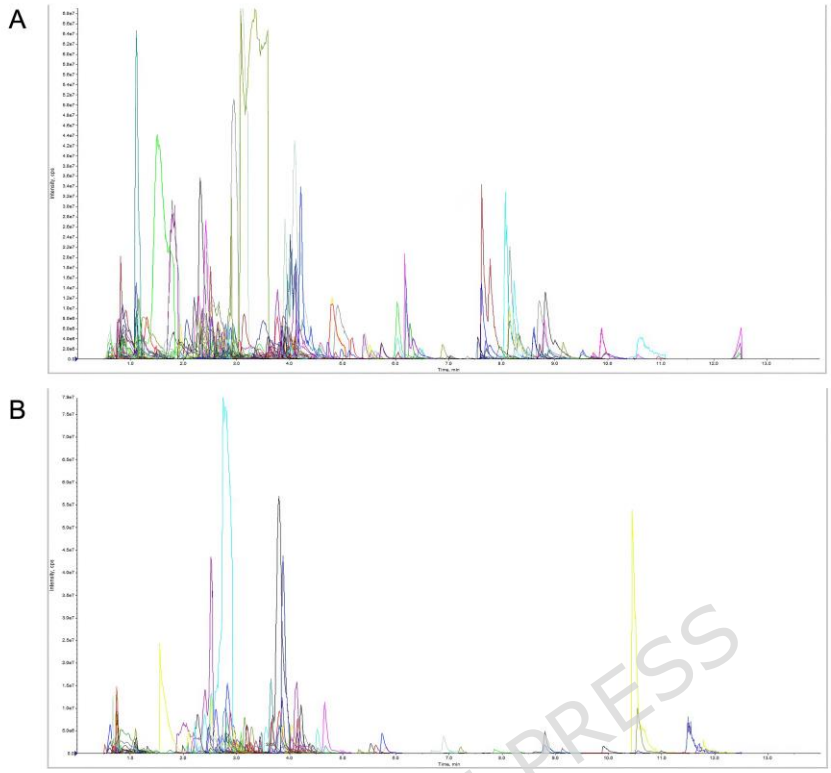

Figure. 3 Multi-peak diagram of MRM metabolite detection. The graph represents the retention time of metabolite detection on the x-axis and the ion current intensity (expressed in cps (counts per second)) of ion detection on the y-axis. Based on the local metabolite database, qualitative and quantitative mass spectrometry analysis was performed on the metabolites in the samples. The multi-peak plot of metabolite detection under MRM mode displays the detectable substances in the samples, where each mass spectral peak of a distinct color represents one detected metabolite.

Table 1. Compounds identified from BKF by UPLC-MS/MS.

Retention time (min)	Molecular mass (Da)	Error	MS Fragmentation	ID	CAS
1.2	116.0	1.1	115.001$[M-H]^-$, 71.102 $[M-H-HCOOH]^-$, 42.326 $[M-H-4H_2O]^-$	Fumaric acid	110-17-8
0.7	117.1	0.9	118.024$[M+H]^+$, 59.049 $[M+H-C_2H_3O_2]^+$	Betaine	107-43-7
0.54	118.0	0.3	116.955$[M-H]^-$, 99.016 $[M-H-H_2O]^-$, 73.114 $[M-H-COCH_3]^-$	Succinic acid	110-15-6
1.4	121.1	0.4	122.20 $[M+H]^+$, 104.099 $[M+H-H_2O]^+$	Phenethylamine	64-04-0
2.9	122.0	0.4	121.028$[M-H]^-$, 79.018 $[M-H-COCH_3]^-$, 53.002 $[M-H-3H_2O-CH_3]^-$,43.018 $[M-H-2H_2O-OCOCH_3]^-$, 41.002 $[M-H-2H_2O-C_2H_5O_2]^-$	4-Hydroxybenzaldehyde	123-08-0
5.4	131.1	1.5	132.203$[M+H]^+$, 113.650 $[M+H-H_2O]^+$, 86.019 $[M+H-HCOOH]^+$,56.517 $[M+H-H_2O-C_2H_2O_2]^+$	6-Aminocaproic acid	60-32-2

4.4	134.0	2.5	133.013 $[M-H]^-$, 115.003 $[M-H-H_2O]^-$, 87.028 $[M-H-HCOOH]^-$, 68.997 $[M-H-H_2O-HCOOH]^-$	L-(-)-Malic acid	636-61-3
4.0	135.1	0.5	136.788 $[M+H]^+$, 78.047 $[M+H-CH_4N_3]^+$	Aminopurine	452-06-2
4.4	137.0	0.6	138.518 $[M+H]^+$, 119.921 $[M+H-H_2O]^+$, 71.743 $[M+H-2H_2O-CH_2O]^+$	Trigonelline	535-83-1
5.6	148.1	0.8	147.045 $[M-H]^-$,129.034 $[M-H-H_2O]^-$, 117.034 $[M-H-CH_2O]^-$	p-Coumaraldehyde	2538-87-6
4.5	150.1	0.2	149.039 $[M-H]^-$,131.099 $[M-H-H_2O]^-$, 120.045 $[M-H-CH_2O]^-$, 91.188 $[M-H-C_2H_3O_2]^-$	D-(-)-Arabinose	10323-20-3
2.7	152.1	0.7	151.016 $[M-H]^-$,133.187 $[M-H-H_2O]^-$, 122.011 $[M-H-CH_2O]^-$, 90.108 $[M-H-C_2H_4O_2]^-$	D-Arabitol	488-82-4
2.9	152.1	0.8	151.060 $[M-H]^-$,133.051 $[M-H-H_2O]^-$, 91.039 $[M-H-H_2O-C_2H_2O]^-$	Xylitol	87-99-0
2.2	153.1	1.0	154.930$[M+H]^+$, 134.158 $[M+H-H_2O]^+$, 91.101$[M+H-H_2O-C_2H_6N]^+$	Dopamine	62-31-7
2.7	152.1	0.7	151.016 $[M-H]^-$,133.187 $[M-H-H_2O]^-$, 122.011 $[M-H-CH_2O]^-$, 90.108 $[M-H-C_2H_4O_2]^-$	D-Arabitol	488-82-4
2.0	188.1	0.3	187.097 $[M-H]^-$,169.086 $[M-H-H_2O]^-$, 151.075 $[M-H-2H_2O]^-$, 141.091 $[M-H-HCOOH]^-$ 123.086 $[M-H-H_2O-HCOOH]^-$, 95.086 $[M-H-C_2H_4O_4]^-$	Anchoic Acid	123-99-9
8.9	192.0	1.8	191.0198$[M-H]^-$,173.008 $[M-H-H_2O]^-$, 145.013 $[M-H-HCOOH]^-$, 129.018 $[M-H-H_2O-HCOOH]^-$, 101.023 $[M-H-C_2H_4O_4]^-$	Citric Acid	77-92-9
10.0	194.1	0.0	193.050 $[M-H]^-$,175.039 $[M-H-H_2O]^-$, 147.044 $[M-H-HCOOH]^-$, 71.013 $[M-H-C_3H_3O_2]^-$, 55.018 $[M-H-H_2O-C_7H_5O_2]^-$	Ferulic acid	1135-24-6
0.9	196.1	0.4	195.05 $[M-H]^-$,177.039 $[M-H-H_2O]^-$, 149.044 $[M-H-HCOOH]^-$	Gluconic acid	526-95-4
2.8	198.1	2.1	197.044 $[M-H]^-$,179.034 $[M-H-H_2O]^-$, 151.003 $[M-H-HCOOH]^-$, 137.023 $[M-H-C_2H_4O_4]^-$	Syringic acid	530-57-4
1.7	202.121	1.0	201.112 $[M-H]^-$,183.102 $[M-H-H_2O]^-$, 155.107 $[M-H-HCOOH]^-$,137.096 $[M-H-H_2O-HCOOH]^-$,109.101 $[M-H-H_2O-HCOOH]^-$, 59.013 $[M-H-C_8H_{14}O_2]^-$	sebacic acid	111-20-6
2.0	208.074	1.7	207.556 $[M-H]^-$,189.002 $[M-H-H_2O]^-$, 145.777 $[M-H-2OCH3]^-$, 42.876 $[M-H-C_8H_9O_3]^-$	Sinapinaldehyde	4206-58-0
7.6	208.074	0.9	207.112 $[M-H]^-$,189.102 $[M-H-H_2O]^-$,171.03 $[M-H-2H_2O]^-$, 146.107 $[M-H-C_2H_5O_2]^-$, 83.023 $[M-H-CH_3-C_6H_5O_2]^-$	Ethyl caffeate	102-37-4
1.5	224.068	0.5	223.060 $[M-H]^-$, 205.050 $[M-H-H_2O]^-$, 177.018 $[M-H-HCOOH]^-$,163.039 $[M-H-C_2H_6O_2]^-$	Sinapic acid	530-59-6
7.7	230.152	0.6	229.144 $[M-H]^-$,211.133 $[M-H-H_2O]^-$, 183.139 $[M-H-HCOOH]^-$, 59.013 $[M-H-C_{10}H_{18}O_2]^-$	Dodecanedioic acid	693-23-2
7.0	256.074	0.7	255.066 $[M-H]^-$,237.055 $[M-H-H_2O]^-$, 151.00 $[M-H-C_8H_8]^-$	Pinocembrin	480-39-7

1.07	260.03	0.3	259.021 $[M-H]^-$,241.011 $[M-H-H_2O]^-$, 213.015 $[M-H-CH_2O_2]^-$,161.009$[M-H-H_2O-H_2PO_3]^-$, 78.958 $[M-H-Glu]^-$	D-Glucose 6-phos-phate	56-73-5
8.8	266.124	0.4	267.021 $[M+H]^+$,249.011 $[M+H-H_2O]^+$, 163.009 $[M+H-C_5H_{13}ON]^+$, 156.01 $[M+H-C_6H_5O_2]^+$	Caffeoylcholine	87189-10-4
7.3	270.053	0.4	271.060 $[M+H]^+$, 253.050$[M+H-H_2O]^+$, 241.050 $[M+H-CH_6O]^+$, 153.018 $[M+H-C_8H_6O]^+$	Apigenin	520-36-5
7.45	272.068	1.6	273.056 $[M-H]^-$, 253.889$[M-H-H_2O]^-$, 135.998 $[M-H-C_8H_8O_2]^-$	Pinobanksin	548-82-3
2.08	284.068	0.4	285.6 $[M+H]^+$, 267.112$[M+H-H_2O]^+$, 249.0$[M+H-2H_2O]^+$, 137.554 $[M+H-C_9H_8O_2]^+$	Acacetin	480-44-4
8.5	286.048	0.6	285.132 $[M-H]^-$, 267.435$[M-H-H_2O]^-$, 249.007$[M-H-2H_2O]^-$, 135.554 $[M-H-C_8H_6O_3]^-$	Kaempferol	520-18-3
6.6	288.063	2.1	287.001 $[M-H]^-$, 269.435$[M-H-H_2O]^-$, 251.712 $[M-H-2H_2O]^-$, 135.554 $[M-H-C_8H_8O_3]^-$	Dihydro-kaempferol	480-20-6
6.7	290.079	2.8	289.000 $[M-H]^-$, 270.000$[M-H-H_2O]^-$, 253.744 $[M-H-2H_2O]^-$, 243.139 $[M-H-HCOOH]^-$, 166.023 $[M-H-C_8H_8O_4]^-$	Catechin	154-23-4
12.6	297.136	0.4	298.067 $[M+H]^+$, 280.112$[M+H-H_2O]^+$, 223.554 $[M+H-2H_2O-2OCH_3]^+$,144.554 $[M+H-C_8H_9O_3]^+$	apoglaziovine	2128-77-0
11.0	302.043	2.4	303.097 $[M+H]^+$, 285.112$[M+H-H_2O]^+$, 231.001$[M+H-4H_2O]^+$, 193.554 $[M+H-C_6H_6O_2]^+$	Quercetin	117-39-5
10.9	314.158	1.8	315.334 $[M+H]^+$, 297.112$[M+H-H_2O]^+$, 248.400$[M+H-2H_2O-OCH_3]^+$, 224.004 $[M+H-C_7H_7O]^+$	Magnocurarine	6801-40-7
10.4	316.058	1.0	315.000 $[M-H]^-$, 297.039$[M-H-H_2O]^-$, 259.024 $[M-H-C_3H_5O]^-$, 243.139 $[M-H-C_7H_5O_4]^-$, 151.003 $[M-H-C_9H_9O_3]^-$	Isorhamnetin	480-19-3
8.4	316.058	0.5	317.667 $[M+H]^+$, 299.112$[M+H-H_2O]^+$, 245.001$[M+H-4H_2O]^+$, 207.554 $[M+H-C_6H_6O_2]^+$, 183.065$[M+H-C_7H_4O_3]^+$	Tamarixetin	603-61-2
11.0	302.0	2.4	303.097 $[M+H]^+$, 285.112$[M+H-H_2O]^+$, 231.001$[M+H-4H_2O]^+$, 193.554 $[M+H-C_6H_6O_2]^+$	Quercetin	117-39-5
10.9	314.2	1.8	315.334 $[M+H]^+$, 297.112$[M+H-H_2O]^+$, 248.400$[M+H-2H_2O-OCH_3]^+$, 224.004 $[M+H-C_7H_7O]^+$	Magnocurarine	6801-40-7
10.4	316.1	1.0	315.000 $[M-H]^-$, 297.039$[M-H-H_2O]^-$, 259.024 $[M-H-C_3H_5O]^-$, 243.139 $[M-H-C_7H_5O_4]^-$, 151.003 $[M-H-C_9H_9O_3]^-$	Isorhamnetin	480-19-3
8.4	316.1	0.5	317.667 $[M+H]^+$, 299.112$[M+H-H_2O]^+$, 245.001$[M+H-4H_2O]^+$, 207.554 $[M+H-C_6H_6O_2]^+$, 183.065$[M+H-C_7H_4O_3]^+$	Tamarixetin	603-61-2
4.6	316.1	0.4	315.198 $[M-H]^-$, 287.060 $[M-H-H_2O]^-$, 269.139 $[M-H-HCOOH]^-$, 135.744 $[M-H-Glu]^-$	Protocatechuicacid-4-glucoside	-
2.8	323.1	0.4	324.777 $[M+H]^+$, 306.112$[M+H-H_2O]^+$, 213.001 $[M+H-H_2O-3OCH_3]^+$,212.554 $[M+H-H_2O-C_3H_9O_3]^+$, 226.766 $[M+H-C_6H_8O_2]^+$, 174.411 $[M+H-C_8H_8O_2N]^+$	Demethylen berberine	25459-91-0

6.0	325.3	0.0	326.004 $[M+H]^+$, 308.332$[M+H-H_2O]^+$, 242.001$[M+H-C_3H_4O_3N]^+$, 116.554 $[M+H-C_{10}H_{18}O_2N_3]^+$	N-Oleoylethanola-mine	111-58-0
4.3	327.1	0.6	328.667 $[M+H]^+$, 310.112$[M+H-H_2O]^+$, 292.001$[M+H-2H_2O]^+$,266.554 $[M+H-2OCH_3]^+$, 191.554 $[M+H-C_8H_9O_2]^+$	Norrisocorydine	475-70-7
6.2	330.1	0.6	329.198 $[M-H]^-$, 313.060 $[M-H-H_2O]^-$, 267.139 $[M-H-2OCH_3]^-$, 244.744 $[M-H-3H_2O-OCH_3]^-$	Di-O-methylquerce-tin	2068-02-2
7.4	337.1	1.2	338.667 $[M+H]^+$, 320.112$[M+H-H_2O]^+$, 306.001 $[M+H-OCH_3]^+$, 237.554 $[M+H-C_5H_8O_2]^+$, 227.554 $[M+H-C_3H_9O_3]^+$, 162.443 $[M+H-C_{11}H_{12}O_2N]^+$	Palmat-rubine	16176-68-4
9.6	337.1	1.6	338.667 $[M+H]^+$, 320.112$[M+H-H_2O]^+$, 307.001 $[M+H-OCH_3]^+$, 227.554 $[M+H-H_2O-C_3H_9O_3]^+$, 226.766 $[M+H-C_6H_8O_2]^+$, 148.411 $[M+H-C_{10}H_{10}O_2N]^+$	columbamine	3621-36-1
9.9	338.1	1.1	337.991 $[M-H]^-$, 319.060 $[M-H-H_2O]^-$, 291.139 $[M-H-HCOOH]^-$, 267.139 $[M-H-C_7H_{11}O_6]^-$	3-O-(E)-p-Coumaroyl quinic acid	87099-71-6
10.9	340.1	0.9	339.003 $[M-H]^-$,321.227 $[M-H-H_2O]^-$, 159.008 $[M-H-Glu]^-$, 123.008 $[M-H-2H_2O-C_9H_8O_4]^-$	Esculin	531-75-9
10.6	341.2	0.9	342.867 $[M+H]^+$, 324.112$[M+H-H_2O]^+$, 311.001 $[M+H-OCH_3]^+$, 231.454 $[M+H-H_2O-2OCH_3]^+$, 230.744 $[M+H-C_6H_8O_2]^+$	Corydine	476-69-7
10.4	341.2	0.2	342.067 $[M+H]^+$, 324.132$[M+H-H_2O]^+$, 311.001 $[M+H-OCH_3]^+$, 194.454 $[M+H-C_7H_5O_2]^+$, 163.554 $[M+H-C_{10}H_{11}O_2N]^+$	bernumidine	-
12.5	342.116	0.4	341.803 $[M-H]^-$,323.227 $[M-H-H_2O]^-$, 161.008 $[M-H-Glu]^-$	Melibiose	585-99-9
12.5	342.1	0.4	341.803 $[M-H]^-$,323.227 $[M-H-H_2O]^-$, 161.008 $[M-H-Glu]^-$	Melibiose	585-99-9
12.6	342.116	1.5	341.803 $[M-H]^-$,323.227 $[M-H-H_2O]^-$, 219.050 $[M-H-H_2O-C_4H_8O_2]^-$,161.045 $[M-H-Glu]^-$	D-(+)-Sucrose	57-50-1
12.7	342.116	0.6	341.097 $[M-H]^-$,323.097 $[M-H-H_2O]^-$, 203.055$[M-H-2H_2O-C_4H_6O_3]^-$, 161.045 $[M-H-Glu]^-$, 101.023$[M-H-C_8H_7O_8]^-$	D-(+)-Trehalose Anhydrous	99-20-7
11.07	342.116	0.6	341.097 $[M-H]^-$,323.097 $[M-H-H_2O]^-$, 203.055$[M-H-2H_2O-C_4H_6O_3]^-$, 161.045 $[M-H-Glu]^-$, 101.023$[M-H-C_8H_7O_8]^-$	Isomaltulose	13718-94-0
11.45	342.116	0.6	341.097 $[M-H]^-$,323.097 $[M-H-H_2O]^-$, 203.055$[M-H-2H_2O-C_4H_6O_3]^-$, 161.045 $[M-H-Glu]^-$, 101.023$[M-H-C_8H_7O_8]^-$	Galactinol	3687-64-7
6.54	342.17	0.9	343.867 $[M+H]^+$, 325.112$[M+H-H_2O]^+$, 313.001 $[M+H-OCH_3]^+$, 247.554 $[M+H-2H_2O-2OCH_3]^+$, 144.744 $[M+H-C_9H_{11}O_4]^+$	Magnoflorine	2141-09-5
6.6	342.288	1.7	343.281 $[M+H]^+$, 325.156$[M+H-H_2O]^+$, 257.001 $[M+H-C_3H_4O_2N]^+$, 172.554 $[M+H-C_7H_{11}O_3N_2]^+$	Cocamidopropyl βine	4292-10-8

3.76	351.147	1.0	352.777 $[M+H]^+$, 334.112$[M+H-H_2O]^+$, 292.994 $[M+H-2OCH_3]^+$, 204.744 $[M+H-C_9H_8O_2]^+$	oxyberberine	549-21-3
2.85	353.126	0.9	354.867 $[M+H]^+$, 339.902$[M+H-H_2O]^+$, 294.566 $[M+H-2OCH_3]^+$, 188.444 $[M+H-C_9H_8O_3]^+$	lennoxamine	95530-38-4
7.6	355.178	0.1	356.004$[M+H]^+$, 236.356$[M+H-4OCH_3]^+$, 218.001 $[M+H-C_8H_{10}O_2]^+$, 164.334 $[M+H-C_{11}H_{14}O_2]^+$	argemonine	6901-16-2
8.4	358.142	0.1	357.007 $[M-H]^-$,339.097 $[M-H-H_2O]^-$, 261.555$[M-H-2H_2O-2OCH_3]^-$, 123.099$[M-H-C_7H_7O_2]^-$, 122.878 $[M+H-C_{13}H_{15}O_4]^+$	Pinoresinol	487-36-5
9.0	367.106	0.6	368.867 $[M+H]^+$, 350.902$[M+H-H_2O]^+$, 308.566 $[M+H-2OCH_3]^+$, 202.509 $[M+H-C_9H_8O_3]^+$	13-deoxychilenine	-
11.0	418.09	0.3	417.082 $[M-H]^-$,399.071 $[M-H-H_2O]^-$, 285.039 $[M-H-C_5H_8O_4]^-$	Juglanin	5041-67-8
2.76	434.121	0.4	433.097 $[M-H]^-$,415.097 $[M-H-H_2O]^-$, 340.055$[M-H-C_6H_5O]^-$, 253.335 $[M-H-Glu]^-$	Naringenin-7-O-glucoside	529-55-5
2.4	442.09	0.1	441.887 $[M-H]^-$, 423.553 $[M-H-H_2O]^-$, 331.123$[M-H-C_6H_6O_2]^-$, 272.881$[M-H-C_7H_5O_5]^-$	Catechin gallate	130405-40-2
4.56	446.121	0.0	447.104 $[M+H]^+$, 429.551$[M+H-H2O]^+$, 267.011 $[M+H-Gal]^+$	Acacetin-7-O-galactosid	-
4.54	448.101	0.1	447.320 $[M-H]^-$, 429.428 $[M-H-H_2O]^-$, 337.106$[M-H-C_6H_6O_2]^-$, 267.011 $[M-H-Glu]^-$	Luteolin-7-O-glucoside	5373-11-5
5.23	448.101	1.1	449.867 $[M+H]^+$, 431.402$[M+H-H_2O]^+$, 269.912 $[M-H-Glu]^+$	Kaempfrol-3-O-glucosid	480-10-4
5.23	448.101	1.1	449.867 $[M+H]^+$, 431.402$[M+H-H_2O]^+$, 269.912 $[M-H-Glu]^+$	Kaempferol-3-O-glucoside	480-10-4
3.87	448.101	1.0	447.101 $[M-H]^-$, 429.034 $[M-H-H_2O]^-$, 354.123$[M-H-C_6H_5O]^-$,267.321$[M-H-Glu]^-$	Kaempferol-3-O-galactoside	23627-87-4
5.67	464.095	0.4	463.456 $[M-H]^-$, 445.332 $[M-H-H_2O]^-$, 354.222$[M-H-C_6H_5O_2]^-$,283.431$[M-H-Gal]^-$	Quercetin-3-O-β-D-Galactoside	482-36-0
6.66	464.095	2.1	465.109 $[M-H]^-$, 445.620 $[M-H-H_2O]^-$, 354.123$[M-H-C_6H_5O_2]^-$, 283.881$[M-H-Glu]^-$	6-Hydroxyluteolin 5-glucoside	-
9.2	464.095	2.0	463.087 $[M-H]^-$, 445.077$[M-H-H_2O]^-$, 343.045$[M-H-C_4H_8O_4]^-$,301.034$[M-H-C_7H_{10}O_5]^-$	Spiraeoside	20229-56-5
2.4	464.095	1.0	465.103 $[M+H]^+$, 447.092$[M+H-H_2O]^+$, 303.566 $[M+H-C_6H_9O_5]^+$, 285.039 $[M+H-Glu]^+$	6-Hydroxykaempferol-7-O-glucoside	-
0.87	464.095	0.6	463.087 $[M-H]^-$, 445.077$[M-H-H_2O]^-$, 343.045$[M-H-C_4H_8O_4]^-$,301.034$[M-H-C_7H_{10}O_5]^-$	Quercetin-3-O-β-D-glucoside	482-35-9
1.0	473.166	0.5	474.173 $[M+H]^+$, 456.163$[M+H-H_2O]^+$, 327.12 $[M+H-C_5H_8NO_4]^+$, 180.088$[M+H-C_{13}H_{13}N_2O_6]^+$	10-Formyl-THF	2800-34-2
1.6	492.127	0.8	493.134 $[M+H]^+$, 475.124$[M+H-H_2O]^+$, 331.081 $[M+H-C_6H_9O_5]^+$	Tricin 7-O-Glucoside	32769-01-0
2.0	504.169	1.4	503.161 $[M-H]^-$, 485.151$[M-H-H_2O]^-$,	D-(+)-Melezitose	597-12-6

			341.108[M-H-Glu]$^-$,323.098[M-H-$C_6H_{13}O_6$]$^-$		
3.0	504.169	1.6	503.161 [M-H]$^-$, 485.150 [M-H-H_2O]$^-$, 457.155 [M-H-HCOOH]$^-$,341.108[M-H-Glu]$^-$	Panose	33401-87-5
3.3	516.127	1.6	515.119[M-H]$^-$, 497.108[M-H-H_2O]$^-$, 471.129[M-H-HCOOH]$^-$,353.087[M-H-$C_9H_7O_3$]$^-$	Cynarin	30964-13-7
5.1	534.101	0.6	533.093 [M-H]$^-$, 515.082 [M-H-H_2O]$^-$, 489.103 [M-H-HCOOH]$^-$,285.039[M-H-$C_9H_{13}O_8$]$^-$, 103.003 [M-H-$C_{21}H_{19}O_{10}$]$^-$	Kaempferol-3-O-(6''-malonyl)-glucoside	81149-02-2
5.6	534.101	0.6	535.117[M+H]$^+$, 517.021[M+H-H_2O]$^+$, 426.441[M+H-$C_6H_5O_2$]$^+$, 270.253 [M+H-malonyl-Glu]$^+$	Luteolin-7-O-(6'-O-malony-β-D-gluco-side	-
6.5	576.127	1.0	577.134 [M+H]$^+$, 559.124[M+H-H_2O]$^+$, 425.087[M+H-$C_8H_7O_3$]$^+$, 109.029 [M+H-$C_{24}H_{19}O_{10}$]$^+$	Procyanidin A2	41743-41-3
6.9	578.142	0.0	577.134 [M-H]$^-$, 559.124 [M-H-H_2O]$^-$, 425.087[M-H-$C_8H_9O_3$]$^-$	Procyanidin B1	20315-25-7
6.7	578.142	0.0	577.134 [M-H]$^-$, 559.124 [M-H-H_2O]$^-$, 425.087[M-H-$C_8H_9O_3$]$^-$	Procyanidin B2	29106-49-8
7.3	578.142	0.6	579.150[M+H]$^+$, 561.139[M+H-H_2O]$^+$, 427.102 [M+H-$C_8H_7O_3$]$^+$, 409.092 [M+H-$C_8H_9O_4$]$^+$	Procyanidin B3	23567-23-9
0.98	594.137	0.8	593.090 [M-H]$^-$, 575.122 [M-H-H_2O]$^-$, 430.345[M-H-$C_9H_7O_3$]$^-$,270.453[M-H-$C_{15}H_{16}O_8$]$^-$	Tiliroside	20316-62-5
7.9	594.158	0.8	595.112[M+H]$^+$, 577.234[M+H-H_2O]$^+$, 486.566 [M+H-$C_6H_5O_2$]$^+$, 281039 [M+H-$C_{11}H_{21}O_{10}$]$^+$	Luteolin 7-O-neohesperidoside	25694-72-8
9.98	594.158	0.8	593.409 [M-H]$^-$, 575.324[M-H-H_2O]$^-$, 484.300[M-H-$C_6H_5O_2$]$^-$,283.544[M-H-$C_{11}H_{19}O_{10}$]$^-$	Kaempferol-3-O-rutinoside	17650-84-9
0.56	594.273	1.6	595.200 [M+H]$^+$, 577.298[M+H-H_2O]$^+$, 541.092[M+H-3H_2O]$^+$,502.122[M+H-3OCH_3]$^+$, 283.039 [M+H-$C_{18}H_{18}O_4N$]$^+$	khyberine	77795-10-9
4.65	596.289	1.9	597.100 [M+H]$^+$, 579.033[M+H-H_2O]$^+$, 543.111[M+H-3H_2O]$^+$,535.122[M+H-2OCH_3]$^+$, 406.221 [M+H-$C_{11}H_{13}O_2N$]$^+$	espinine	26137-40-6
12.12	608.289	0.6	609.200 [M+H]$^+$, 591.100[M+H-H_2O]$^+$, 516.122[M+H-3OCH_3]$^+$,374.090 [M+H-$C_{13}H_{17}O_3N$]$^+$	Berbamine	478-61-5
12.4	610.153	0.4	611.294[M+H]$^+$, 593.255[M+H-H_2O]$^+$, 502.222 [M+H-$C_6H_5O_2$]$^+$, 286.546 [M+H-$C_{12}H_{21}O_{10}$]$^+$	Quercetin-3-O-neo-hesperide	117611-67-3
10.56	610.153	0.5	609.145 [M-H]$^-$, 591.135[M-H-H_2O]$^-$, 463.087[M-H-$C_6H_{11}O_4$]$^-$,301.034[M-H-$C_{12}H_{21}O_9$]$^-$	Quercetin-3-O rutinoside	153-18-4
10.0	622.304	0.1	623.312 [M+H]$^+$, 607.280[M+H-H_2O]$^+$, 594.285 [M+H-CH_2N]$^+$, 580.269[M+H-C_2H_4N]$^+$	Isotetrandrine	477-57-6
2.7	666.222	0.8	665.214 [M-H]$^-$, 647.203[M-H-H_2O]$^-$, 503.161[M-H-Glu]$^-$,485.150[M-H-$C_6H_{13}O_6$]$^-$	1,1-Kesto-tetraose	13133-07-8
6.6	866.2	0.8	865.198 [M-H]$^-$, 847.187[M-H-H_2O]$^-$, 755.161[M-H-$C_6H_7O_2$]$^-$,713.150[M-H-$C_8H_9O_3$]$^-$	Procyanidin C1	37064-30-5

5.7	866.2	0.8	865.198 $[M-H]^-$, 847.187$[M-H-H_2O]^-$, 755.161$[M-H-C_6H_7O_2]^-$,713.150$[M-H-C_8H_9O_3]^-$	Procyanidin C2	37064-31-6
6.7	866.2	2.1	467.103 $[M+H]^+$, 849.092$[M+H-H_2O]^+$, 756.100 $[M+H-C_6H_7O_2]^+$, 714.103 $[M+H-C_8H_9O_3]^+$	Arecatannin B1	79763-28-3
9.5	1154.3	0.3	1153.245 $[M-H]^-$, 1135.235$[M-H-H_2O]^-$, 1043.208$[M-H-C_6H_9O_2]^-$,1001.198$[M-H-C_8H_{11}O_3]^-$	Cinnamtannin B2	88038-12-4

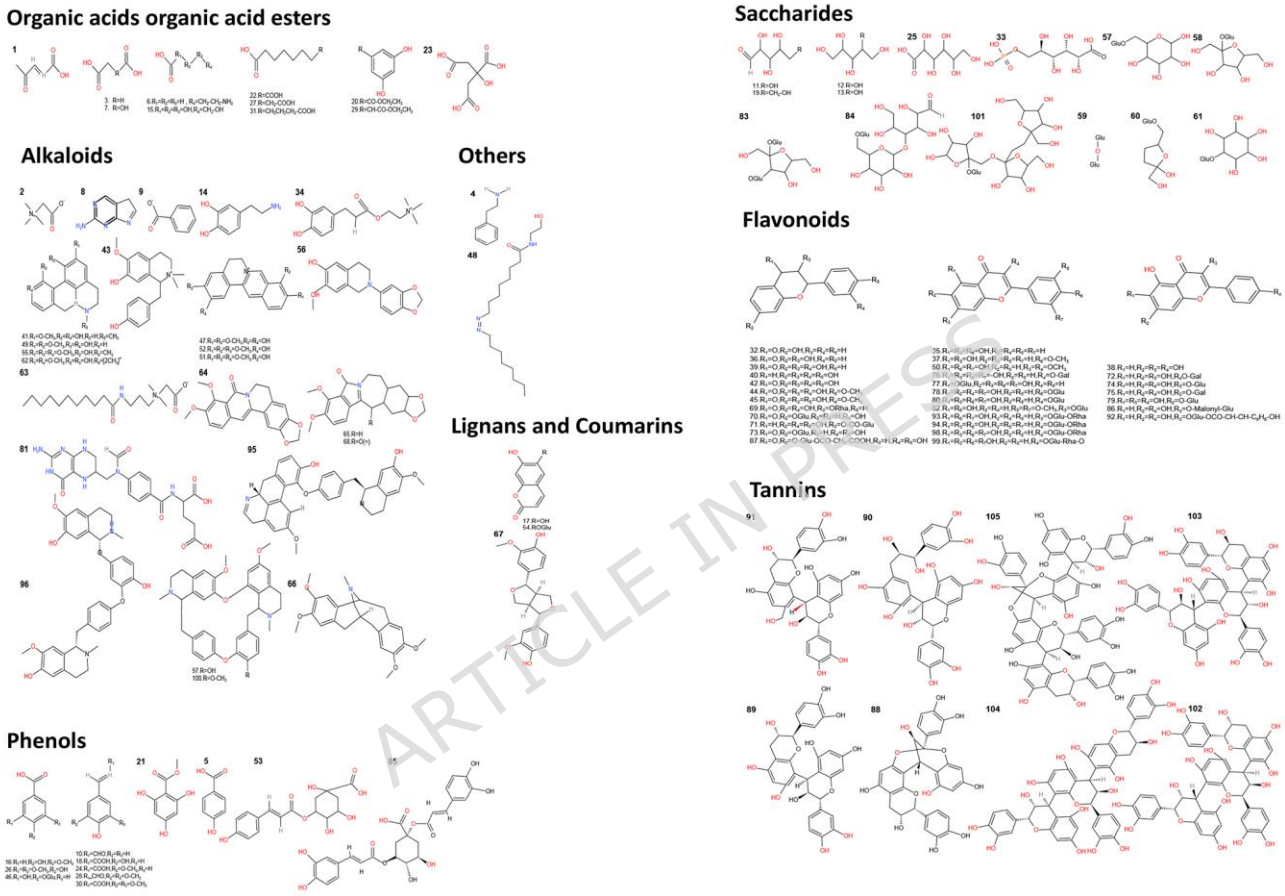

Figure. 4 The 2D structures of components identified in BKF.

2.2. Network pharmacology analysis

All alkaloids, except 10-formyl-THF, met the five principles of Lipinski. Moreover, most alkaloids exhibited ideal water solubility and tissue absorption properties. Caffeoylcholine, apoglaziovine, magnocurarine, norisocorydine, palmatrubine, columbamine, corydine, bernumidine, magnofolrine, oxyberberine, lennoxamine, argemonine, and 13-deoxychilenine exhibit appropriate physical and chemical spatial ranges for oral bioavailability. The bioavailabilities of the fundamental components were all 0.55.

We primarily focused on the toxicity of the alkaloids. Out of the 24 alkaloids studied, none showed hepatotoxicity or inhibitory effects on hERG1 (human ether-a-go-go gene1). However, we found that caffeoylcholine, norisocorydine, palmatrubine, columbamine, corydine, Kyberine, and berbamine did inhibit hERG2 (human ether-a-go-go gene2). Hepatotoxicity and hERG1 inhibition were prioritized as exclusion criteria because chronic administration of toxic compounds is unacceptable for AS management. All 24

alkaloids met Lipinski's Rules, ensuring favorable oral bioavailability a critical requirement for anti-inflammatory agents intended for oral administration. PkCSM predictions showed that 7 alkaloids had high Caco-2 permeability, indicating good GI absorption. The remaining 5 alkaloids had moderate permeability but were retained due to their water solubility, which may enable local anti-inflammatory effects in the gut.

We categorized the 24 alkaloids into two groups based on their lipophilic partition coefficient (LogP value) and the available literature. The first group, FSA, included Caffeylcholine, apoglaziovine, demethyleneberberine, norisocorydine, palmatrubine, columbaminine, corydine, bernumidine, magnoflorine, cocamidopropyl betaine, OBB, lennoxamine, argemonine, 13-deoxychilenine, Khyberine, Espinine, berbamine, and isotetrandrine. The second group, WSA, included betaine, magnocurarine, aminopurine, trigonelline, dopamine, and 10-formyl-THF.

A total of 583 ABK targets and 4,481 human AS targets were obtained (Figure 5). We identified 366 intersecting targets. Then, we performed GO functional and KEGG pathway enrichment analysis for potential anti-AS targets in the TA, FSA, WSA, and OBB groups (Figures 6, 7 , 8, and 9, respectively).

To elucidate the functional differentiation and potential synergy among different alkaloid subsets in BKF, we analyzed the predicted targets and enriched pathways for TA, FSA, WSA, and OBB (Figures 6–9). Analysis of shared targets revealed enrichment in inflammatory response regulation, lipid metabolism, and cell pyroptosis, indicating that all subsets converge on core pathways in AS progression. FSA-specific pathways included "cholesterol transport" and "oxidative stress response", consistent with their lipophilic nature, which supports cell membrane penetration and intracellular lipid regulation. Conversely, WSA-specific pathways, such as "endothelial barrier protection" and "antibacterial response", align with their high aqueous solubility, suggesting action on extracellular or membrane-associated targets. OBB, as a key monomer, was found to significantly contribute to the lipid-regulating and anti-inflammatory effects observed in the FSA subset. Finally, the target profile of TA integrated both FSA- and WSA-specific targets, demonstrating its synergistic role across multiple AS-related processes.

The significant enrichment of three core KEGG pathways ($p < 0.01$) in all four groups confirms their shared anti-AS potential. First, the enrichment of the TLR4/NF-κB signaling pathway in all groups suggests that inhibiting LPS-mediated inflammation is a universal mechanism of BKF alkaloids. Second, the JAK-STAT3 pathway, crucial for macrophage polarization, was similarly enriched, implying that lipophilic alkaloids are its main regulators. Third, the enrichment of the NLRP3 Inflammasome Activation pathway specifically in the TA, FSA, and OBB groups implies a more dominant role for FSA and OBB in inhibiting the cell pyroptosis involved in AS plaque necrosis.

This comparative analysis clarifies that FSA (and OBB) dominates lipid metabolism and pyroptosis regulation, while WSA specializes in endothelial protection, and TA integrates the advantages of both subsets. These findings not only validate the rationality of grouping alkaloids by solubility but also provide a clear "target-pathway" basis for interpreting the in vitro results, such as OBB's stronger inhibitory effect on TLR4/pSTAT3 than WSA, and FSA's superior regulation of caspase-11 compared to TA.

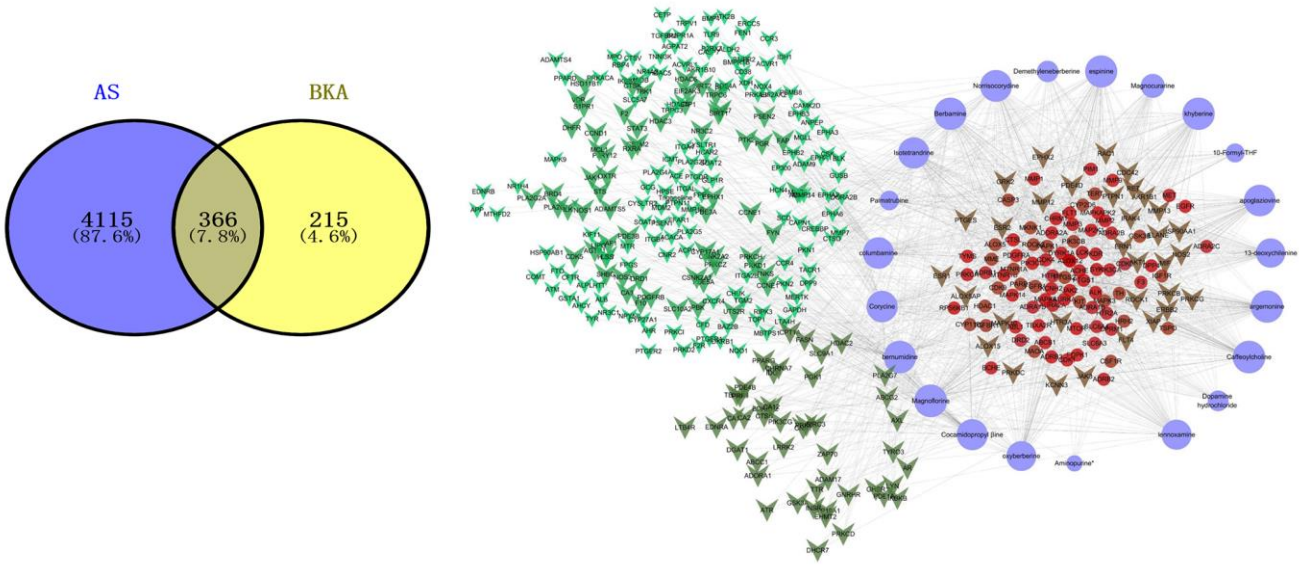

Figure. 5 Venn analysis of the interaction targets and the visual network analysis diagram of ABK and AS.

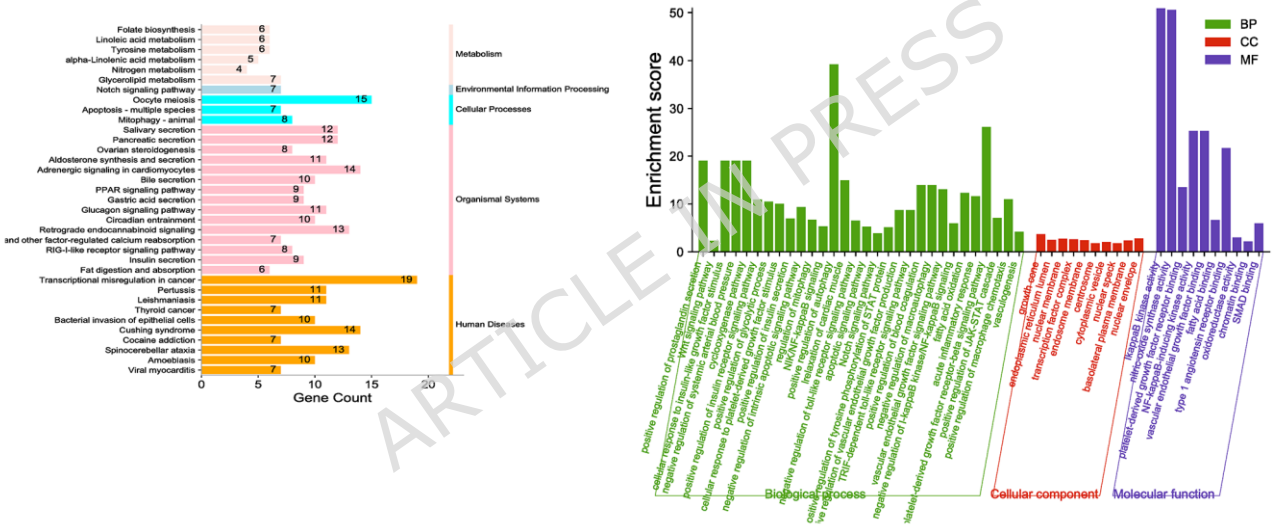

Figure. 6 KEGG pathway and GO functional enrichment analysis of ABK (TA) total targets. Pathway diagram adapted from KEGG [24],[25],[26].

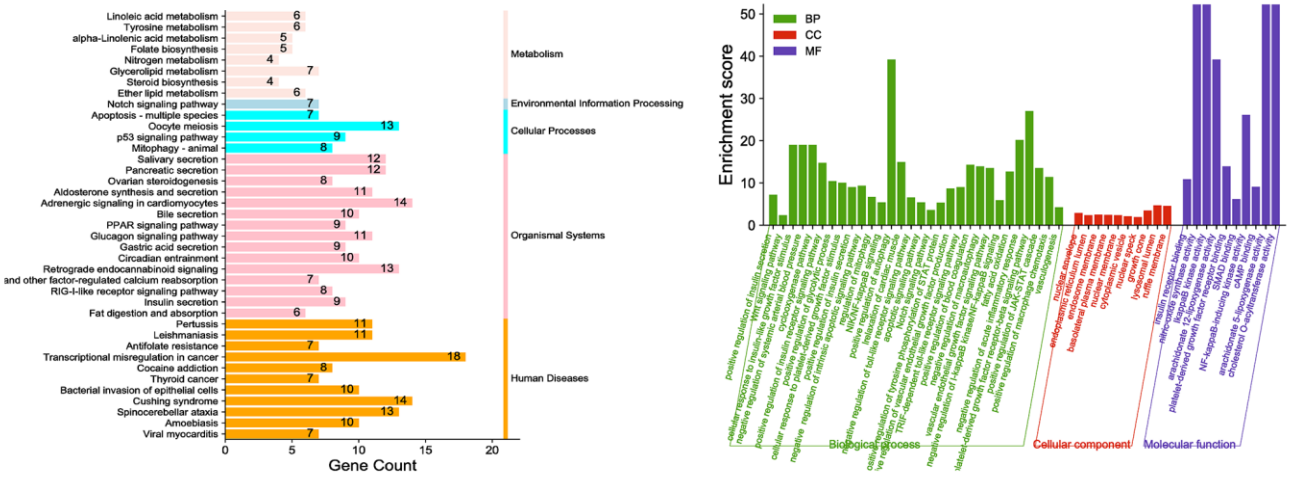

Figure. 7 KEGG pathway and GO functional enrichment analysis of FSA total targets. Pathway diagram adapted from KEGG [24],25],[26].

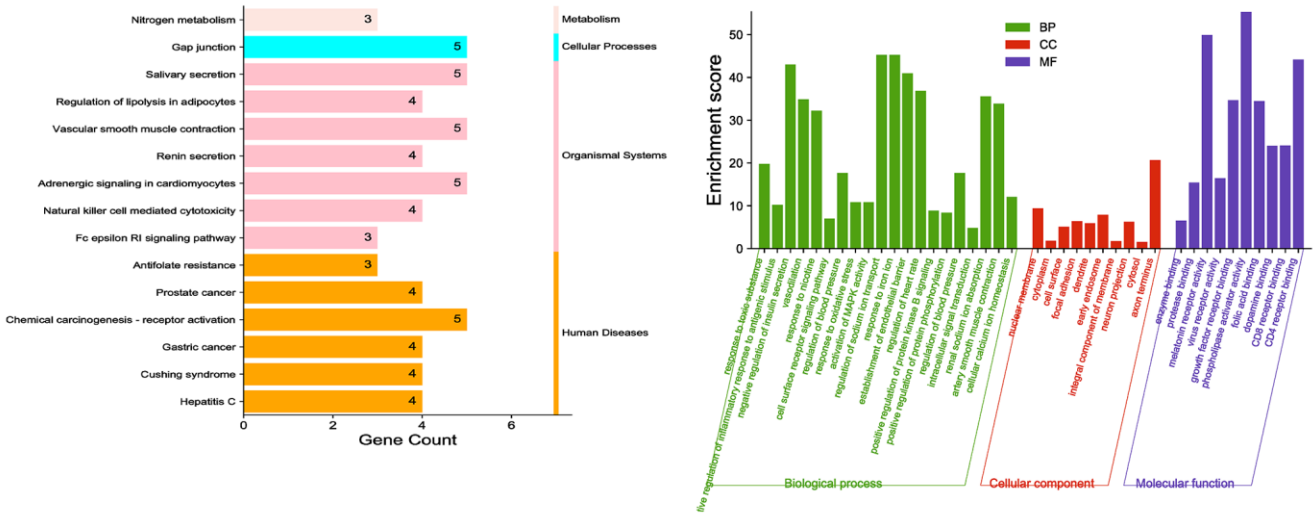

Figure. 8 KEGG pathway and GO functional enrichment analysis of WSA total targets. Pathway diagram adapted from KEGG [24],[25],[26].

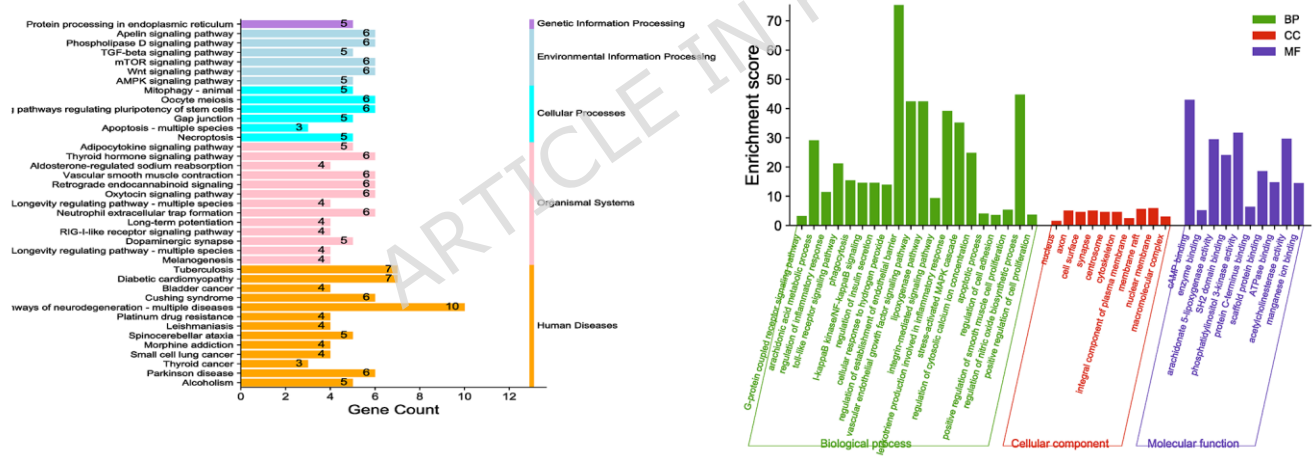

Figure. 9 KEGG pathway and GO functional enrichment analysis of OBB total targets. Pathway diagram adapted from KEGG [24],[25],[26].

2.3. Effects of ABK and OBB on pyroptosis in LPS-stimulated RAW264.7 cells

In LPS - exposed RAW264.7 cells, mouse caspase - 11 acts as the key target of LPS, triggering a non - classical pyroptosis pathway [27]. Once activated, caspase - 11, in conjunction with gasdermin D (GSDMD), sets off a cascade that activates pro - inflammatory cytokines such as IL - 1β and IL - 18 [28]. To assess the anti - pyroptosis properties of ABK and OBB, we employed ELISA to quantify the levels of caspase - 11, caspase - 1, IL - 1β, and IL - 18 in the cell supernatants. As shown in Figure 10, the LPS group exhibited significantly elevated levels of these factors (caspase - 11 in Figure 10A, caspase - 1 in Figure

10B, IL - 1β in Figure 10C, and IL - 18 in Figure 10D) compared to the control group. In contrast, both ABK and OBB treatment led to a notable reduction in the levels of caspase - 11, caspase - 1, IL - 1β, and IL - 18. This reduction was dose - dependent, with lower levels corresponding to higher concentrations of ABK and OBB.

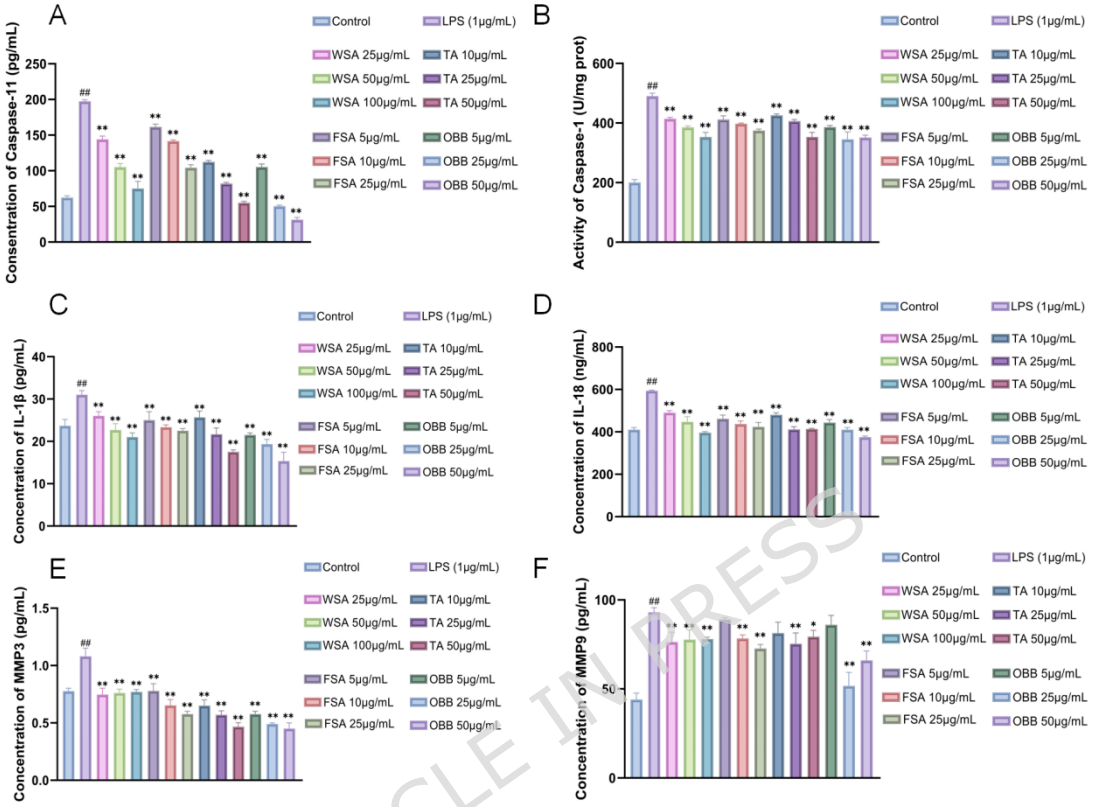

Figure. 10 Effects of ABK and OBB on LPS-stimulated Extracellular Caspase-11 in RAW264.7. The levels of caspase-11 (A), caspase-1 (B), IL-1β (C), IL-18 (D), MMP3 (E), and MMP9 (F) are presented. ##P<0.01 vs. Control group; n=3, **P<0.01, *P<0.05 vs. LPS group.

2.4. Effects of ABK and OBB on TLR4-induced inflammation in LPS-stimulated RAW264.7 cells

To confirm the anti-inflammation effects of ABK and OBB, we detected the levels of TLR4, pSTAT3 and TLR4 expressions by Western blot, respectively. As shown in Figure 11, the levels of TLR-4 expression in the LPS groups significantly increased. ABK and OBB inhibited the level of TLR-4 expression, especially in the OBB group.

The levels of p-STST3 expression in the LPS groups were increased. The inhibitory effects of the WSA and OBB groups were stronger. Figure 10E clearly shows that the OBB group had a more pronounced effect in inhibiting the levels of MMP3 expression compared to other groups. For the protein levels of MMP9, there was a dose-dependent relationship only in the WSA group. Figure 11 demonstrates that the FSA, WSA, TA, and OBB groups all decreased the expression of GSDMD in LPS-stimulated RAW264.7 cells. Additionally, there was a significant elevation in the levels of MMP3 and MMP9 in the cell supernatant in the LPS groups compared to the normal groups. On the other hand, the levels of MMP3 and MMP9 were significantly reduced in the ABK and OBB groups compared to the LPS groups.

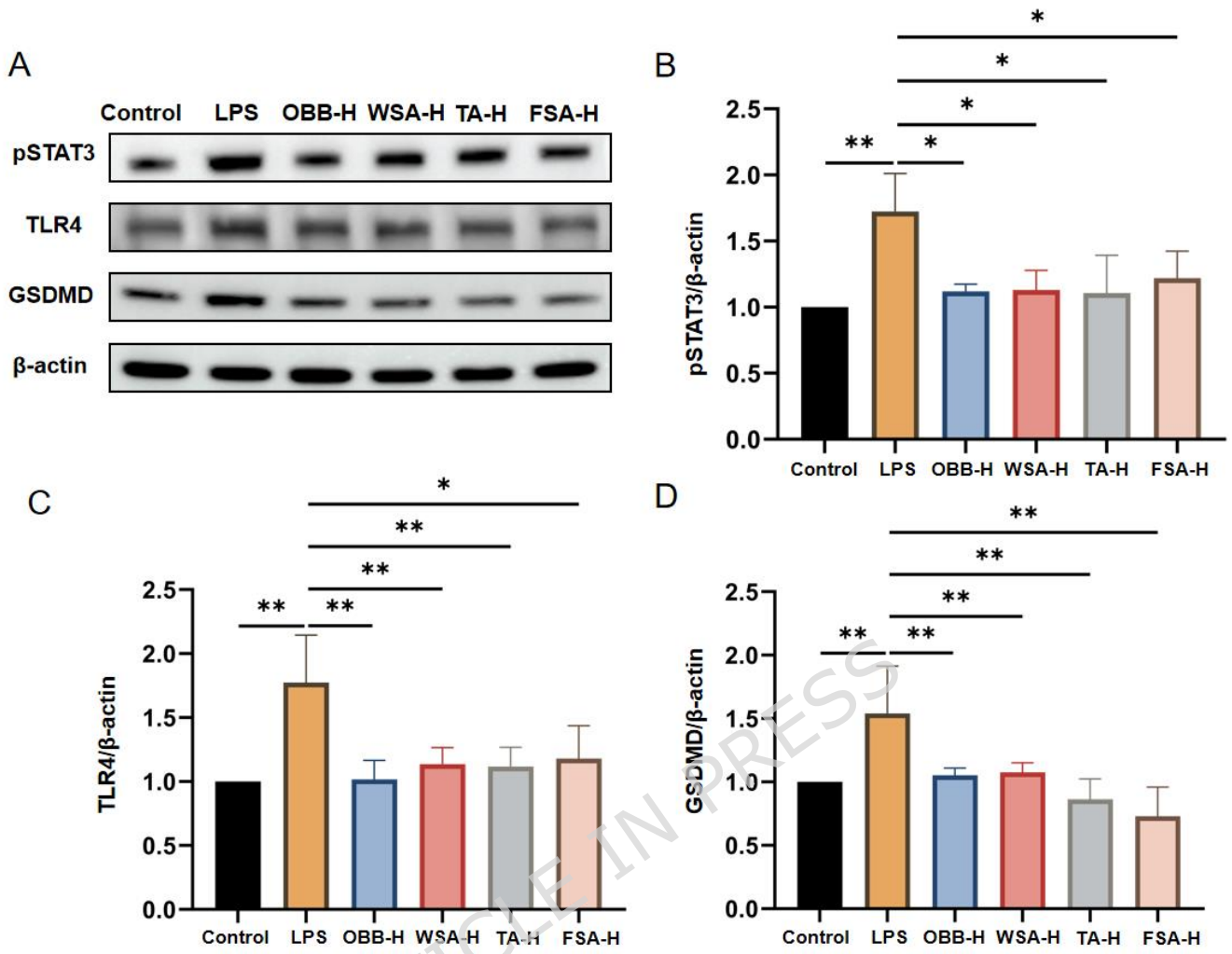

Figure. 11 Effects of ABK and OBB on LPS-stimulated protein expression in RAW264.7. Western blot detected protein expression in RAW264.7 (A). Expression level of p-STAT3 in RAW264.7 (B). Expression level of TLR4 in RAW264.7 (C). Expression level of GSDMD in RAW264.7 (D). Relative protein level was calculated. n=3, **P<0.01, *P<0.05.

These results indicate that the four natural extracts in this study have good inhibitory effects on the inflammatory response caused by TLR-4 activation, which may play an anti-inflammatory role. Meanwhile, these can inhibit the expression of MMP3 and MMP9 to varying degrees, which may have a protective effect on the vascular endothelium. In addition, natural extracts can inhibit the phosphorylation level of STAT3 to some extent, which may participate in the occurrence and development of many STAT3-related diseases and play more pharmacological functions.

3. Discussion

In UPLC-MS/MS analysis of BKF, 105 secondary metabolites were identified, comprising flavonoids, polyphenols, alkaloids, sugars, saponins, coumarin, lignin, organic acids, and other components. Specifically, 24 alkaloids were identified, with 18 being FSA and 6 being WSA. The 24 alkaloids were subjected to analysis using TCMSP database, and pkCSM server, which revealed that ABK exhibited significant medicinal value. Further, prediction through KEGG and GO function enrichment analysis suggested that the pharmacological action of FSA was associated with lipid regulation, while the pharmacological action of WSA was linked to antibacterial and anti-external stimulation. Both types of alkaloids also showed potential anti-inflammatory effects. Moreover, FSA, WSA, TA, and OBB were observed to significantly decrease the secretion of extracellular Caspase-11, IL-

18, and IL-1β, along with the expression of GSDMD protein in mouse macrophages stimulated by LPS. These compounds also reduced the activity of intracellular Caspase-1, inhibiting the non-classical pathway cell death induced by LPS. Additionally, they exhibited varying degrees of inhibition toward the initiation of TLR-4-related inflammation, along with the expression of MMPs and activation of the JAK-STAT3 pathway. Hence, it is suggested that ABK and OBB may not only possess anti-pyroptosis and anti-inflammatory effects but also offer protection to the vascular endothelium. These findings are generally consistent with the results predicted via network pharmacological analysis.

In 2010, Wang et al. [3] conducted a preliminary study on the compositional analysis of BKF using a basic colorimetric method. Subsequently, no further research on the composition of BKF has been published. UPLC-MS/MS has been extensively employed in the study of natural products due to its numerous advantages, including rapid analysis, efficient separation, high resolution and sensitivity, precise quantification, and rapid identification [29]. Our research findings address the existing research gap in this area.

Since its proposal by Hopkin in 2007, network pharmacology has been employed to elucidate the mechanism of action of traditional Chinese herbal medicine, thereby overcoming the limitation of treating a single disease with a solitary component. Natural products exhibit complex biological activities and are frequently employed in the treatment of diseases within traditional Chinese medicine. The distinctive biological activities of natural products are demonstrated through the complex and specialized interaction with organisms in traditional Chinese medicine. After entering the human body, natural products exhibit diverse modes of action: direct interaction with specific targets, generation of metabolites that subsequently target specific entities, modulation of endogenous substances to exert an indirect effect, or interaction with various targets to elicit synergistic effects.

Berberis alkaloids exhibit a broad spectrum of pharmacological effects, such as anti-inflammatory, antibacterial, antiviral, antidiarrheal, antihypertensive, antihypoxic, hypoglycemic, hypolipidemic, and anti-tumor properties [3,6,8]. Recent research on the water extract of BKF has highlighted its ability to dilate blood vessels, lower blood pressure, regulate blood lipid levels, and combat atherosclerosis (AS) [7,30]. Being a natural medicine, BKF contains numerous chemical components and exhibits complex pharmacological effects; However, its mechanism of action in diseases has not been fully elucidated. This study utilized network pharmacology to systematically elucidate the anti-AS properties of 24 alkaloids in BKF, enrich and analyze the protein targets predicted by these active components, and describe the direct relationship between the components and their targets by integrating signaling pathways. The KEGG pathway analysis in our study revealed that lipid metabolism, cell apoptosis, and mitochondrial autophagy were the primary pathways of ABK. Lipid metabolism disorder is a significant risk factor for AS [31]. Studies [15,32-34] have demonstrated a close relationship between cell apoptosis, mitochondrial autophagy, and AS. He et al. [35] found that the activation of AMPK enhanced mitochondrial autophagy via the PINK1/Parkin pathway induced by the endogenous ligand APJ (apelin-13). This led to the proliferation of human aortic vascular smooth muscle cells and the development of atherosclerotic lesions in ApoE-/- mice. Additionally, it has been shown that NIX-mediated mitochondrial autophagy inhibits ox-LDL-induced apoptosis in AS macrophages [38].

The pharmacological effects of ABK, as revealed in the GO analysis, encompass several aspects: regulation of inflammatory reactions, the occurrence and development of diabetes, regulation of programmed cell death and blood pressure, protection of vascular endothelium, and, thrombosis and angiogenesis. Following treatment with intestinal flora, OBB, a metabolite of berberine, exerts its excellent anti-inflammatory effect through the TLR4-MyD88-NF-kappa B inflammatory pathway [37,38]. Moreover, it regulates

blood glucose by modulating the PI3K/Akt and Nrf2 signaling pathways [42] and treats rat fatty liver [49]. Magnoflorine [41-43] possesses antibacterial, hypoglycemic, antihypertensive, and anti-inflammatory effects, which are closely associated with the development of AS. Demethylene berberine hydrochloride is synthesized through the primary metabolism of berberine in the liver [44]. Zuo et al [45] suggested that demethylene berberine hydrochloride was the most potent topoisomerase I inhibitor among several berberine derivatives. Tetrandrine has been shown to decrease glycine levels, thus protecting cells from oxidative stress and reducing the severity of inflammation and pain. Betaine exhibits a range of biological activities, including regulation of lipid metabolism, glucose-lowering effects, anti-inflammatory properties, and neuroprotection [48]. Through network pharmacology analysis of the multi-target pathways of ABK's active components, it was observed that numerous active components in ABK act on AS through various channels, revealing the interaction of multiple natural components and targets. This approach can better elucidate the mechanism by which specific components of ABK treat diseases by targeting particular pathways, thereby providing evidence for the selection of pharmaceutical components during drug research and development. The findings of this network pharmacology study align with the known pharmacological effects of individual alkaloids, indicating the reliability of target prediction. Furthermore, the limited reports on certain alkaloids and potential targets beyond those mentioned offer insights for future investigations into the active components of ABK and their mechanisms of action.

AS is a chronic inflammatory disease predominantly affecting the aortic wall. It is characterized by lipid deposition, plaque formation due to inflammatory cell accumulation beneath the aortic intima, and vascular hardening and narrowing caused by decreased elasticity. Previous studies [47-50] have primarily focused on apoptosis, autophagy, oxidative stress, and inflammation in the pathogenesis of AS. However, the study of pyroptosis has recently emerged as a new area of interest in AS. Studies [11,51-53] have shown that macrophages within plaques can experience apoptosis, pyroptosis, and ferroptosis. In advanced AS plaques, macrophages comprise up to 50% of the deceased cells [10]. Their death can exacerbate vascular inflammation, contribute to the formation and expansion of necrotic cores, and increase plaque instability [54]. The occurrence of pyroptosis is reliant on pro-inflammatory caspases [9]. The role of GSDMD in mediating pyroptosis in immune macrophages was first reported in 2015 [55,58]. Subsequently, it was found that GSDMD can induce pyroptosis by forming pores on the cell membrane [56,57]. In 2017, it was revealed that GSDMD served as the primary channel for the release of IL-1 during pyroptosis [59]. The mechanism of protease cleavage of GSDMD and its crucial role in tumor immunity was elucidated in 2020. These findings have laid the groundwork for advancing medicine development, clinical diagnosis, and treatment [60-62]. Macrophages are widely recognized as the primary producers of IL-1β and IL-18, two crucial substrates that activate caspase-1 and contribute to the inflammation associated with AS. The occurrence and development of AS involve the activity of caspase-1 and inflammatory factors stimulated by various factors.

The commencement of non-classical pyroptosis in mouse cells involves the activation of Caspase-11 by LPS. This, in turn, cleaves the N-terminus of GSDMD and simultaneously activates Caspase-1, leading to the maturation of IL-1β and IL-18. Our findings concerning pyroptosis demonstrated a clear disparity between the control group and the LPS-treated group, indicating the successful induction of non-classical pyroptosis in RAW264.7 macrophages by LPS. Subsequent interventions with ABK and OBB significantly reduced the levels of Caspase-11, caspase-1, IL-1β, IL-18, and the expression of GSDMD. Notably, at the same dose (25 μg/ml), the inhibitory effects of the four intervention drugs on these proteins were compared. The strongest inhibitory effect at a concentration of 25 μg/ml was OBB, followed by FSA, WSA, and TA. This may be attributed to

the high purity of the OBB monomer (exceeding 98%), which enables a more targeted drug effect compared to the other extracts.

Inflammation is a pivotal factor in the development of atherosclerotic (AS) plaques. The onset of AS is triggered by vascular endothelial injury, lipid metabolism dysregulation, and abnormal hemodynamics. Additionally, blood - flow - induced inflammatory changes in endothelial cells during AS also contribute to the disease process [63].

Once activated, endothelial cells secrete a cascade of inflammatory factors, which attract immune cells to the arterial wall and initiate an inflammatory response. This complex process involves macrophages, T and B lymphocytes, dendritic cells, vascular smooth muscle cells, ionic liquids, adhesion molecules, and tumor necrosis factor. As a result, a significant quantity of low - density lipoproteins (LDLs) are oxidized into oxidized LDLs (ox - LDLs), which then accumulate on the inner vascular walls [64]. Monocytes differentiate into macrophages, which engulf the deposited ox - LDLs and transform into foam cells [65]. Pro - inflammatory monocytes preferentially accumulate in AS plaques and adhere to cytokine - stimulated endothelial cells [23]. In the advanced stage of AS, a large number of macrophages and inflammatory factors infiltrate the vessel wall. These cells secrete matrix metalloproteinases (MMPs) that break down the extracellular matrix collagen fibers of the plaque. This degradation can lead to plaque rupture, bleeding, and thrombosis. Toll - like receptor 4 (TLR4) is a crucial gene involved in mediating inflammation and promoting cellular lipid accumulation [65]. As reported [66], high - level expression of TLR4 can activate the JAK2/STAT3 pathway. Elevated expression of MMP3 and MMP9 is associated with AS - related vascular damage.

ABK and OBB exhibit both anti-inflammatory and antioxidant properties [27,67]. Our findings demonstrated that ABK and OBB effectively suppressed the expression of TLR-4 in LPS-induced RAW264.7 cells. OBB exhibited the most potent inhibitory effect, followed by WSA and TA.

Activated p-STAT3 mediates signal transmission from various cytokines and growth factors to the nucleus, influencing target gene transcription, regulating cell functions, and contributing to the development of cardiovascular diseases and other conditions [68]. This study demonstrated that ABK and OBB suppressed the phosphorylation level of STAT-3 protein in LPS-induced RAW264.7 cells. The effect of OBB was significantly greater than that of the TA and WSA groups, with no significant difference observed between the TA and WSA groups. This result may be attributed to the inhibitory effect of both FSA and OBB on the overexpression of TLR-4, consequently suppressing the initiation of the JAK2/STAT3 pathway.

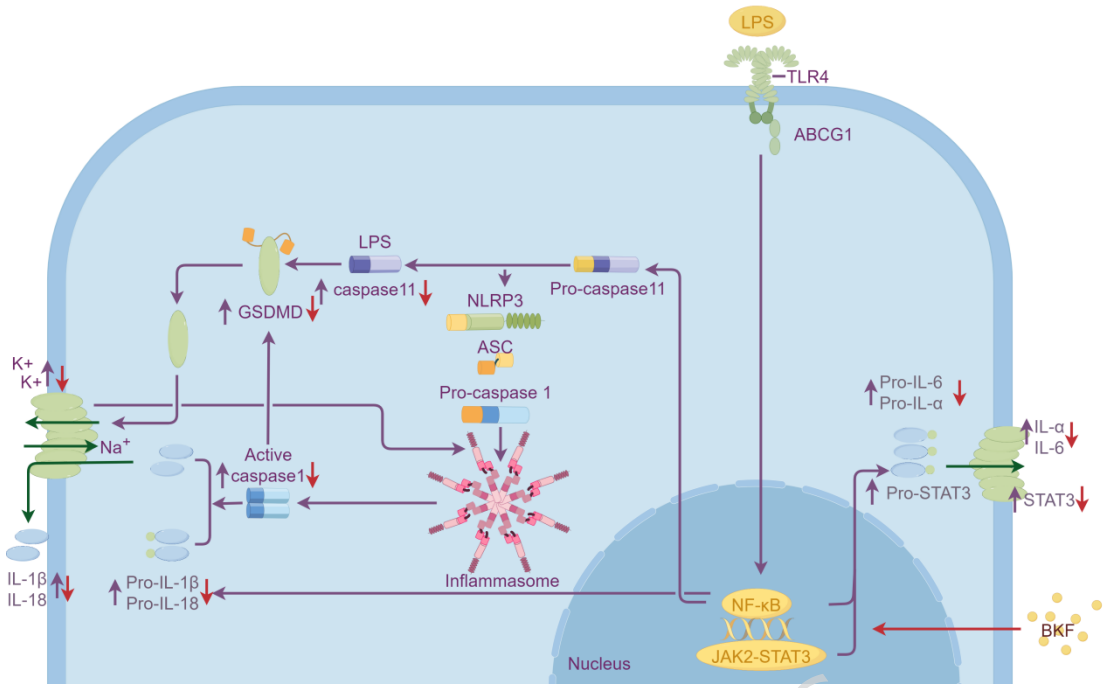

Figure. 12 Potential role of BKF in pyroptosis. (by Figdraw 2.0). BKF was observed to significantly decrease the secretion of extracellular Caspase-11, IL-18, and IL-1 β , along with the expression of GSDMD protein in mouse macrophages stimulated by LPS. These compounds also reduced the activity of intracellular Caspase-1, inhibiting the non-classical pathway cell death induced by LPS. Additionally, they exhibited varying degrees of inhibition toward the initiation of TLR-4-related inflammation, along with the expression of MMPs and activation of the JAK-STAT3 pathway.

To enhance the translational relevance and contextualization of our study, we have integrated recent global research findings. A 2023 Iranian randomized controlled trial demonstrated that Berberis vulgarisfruit extract significantly lowered TC and LDL-C in patients with metabolic syndrome, yet explicitly highlighted the need to characterize the specific active components responsible for lipid regulation—a gap directly addressed by our identification of 24 alkaloids in Berberis kaschgarica[69]. A 2022 U.S. study confirmed that the major alkaloid berberine suppresses macrophage foam cell formation and atherosclerosis progression in mice, but noted the absence of data on other alkaloid subtypes and their synergistic effects, thereby justifying our comparative analysis of FSA, WSA, TA, and OBB both computationally and experimentally [70] And Singh et al. (2023) identified 16 alkaloids in Berberis aristata and reported their anti-inflammatory effects via TLR4 inhibition, but "did not explore lipid-soluble vs. water-soluble subgroups or pyroptosis regulation" [71]. We contrasted this with our results (24 alkaloids, subgroup-specific pathways: FSA for lipid metabolism, WSA for endothelial protection) to highlight BK's richer alkaloid diversity and our more comprehensive mechanistic exploration.

Our results also showed that ABK and OBB effectively inhibited the expression of MMP3 and MMP9 in LPS-induced RAW264.7 cells. However, the effects of different doses of ABK and OBB on MMP3 and MMP9 were uncertain and needed further investigation. This may indicate a cellular stress response to the high expression of MMPs. Although ABK and OBB had varying degrees of inhibitory effects on this response, their action trends were inconsistent both between each other and within the group, as well as across different dosage ranges.

However, the preliminary identification of the 24 alkaloids in this study was accomplished by comparing the retention time, molecular ion peaks, and secondary fragment

ion information obtained via UPLC-MS/MS with the standard spectra from the NIST database and relevant research literatures. This study has not yet used authentic reference standards for further verification of the 24 alkaloids, which may pose a potential risk of qualitative deviation for some components. In subsequent studies, we will purchase or prepare the corresponding reference standards and combine them with methods such as HPLC-DAD to further confirm the structure and content of the alkaloids, thereby improving the accuracy of the results. Network pharmacology predicted 366 anti-AS targets for BKF alkaloids, but we did not validate their in vivo efficacy using animal models. In vivo studies investigating plaque regression, lipid metabolism regulation, and long-term safety are essential to translate our in vitro findings to potential clinical applications. Despite their notable adverse effects on the stress response caused by LPS, there are additional related issues to be addressed, namely the potential simultaneous inhibition of stress, promotion of TIMP-1, and inhibition of MMPs, which require further discussion.

4. Materials and Methods

4.1. Sample preparation for UPLC-ESI-MS/MS

Berberis kaschgarica fruit (BKF) samples were procured from local herbal markets in Kashgar, Xinjiang, China. Professor Palida Abulizi of the School of Pharmacy at Xinjiang Medical University authenticated the botanical identity of the specimens. Freeze - dried BKF samples underwent pulverization at 30 Hz for 1.5 minutes in a mixer mill with zirconia beads. Exactly 100 mg of the resultant powder was accurately weighed and extracted with 1.2 mL of 70% aqueous methanol at 4°C overnight. Following centrifugation at 10,000 g for 10 minutes, the extracts were loaded onto a CNWBOND carbon - GCB solid - phase extraction column (ANPEL, Shanghai, China). The eluates were then filtered through an SCAA - 104 filter (ANPEL, Shanghai, China). The purified extracts were subsequently subjected to analysis using a UPLC - ESI - MS/MS system, consisting of a Shim - pack UPLC SHIMADZU CBM30A for UPLC separation and an Applied Biosystems 6500 Q TRAP for tandem mass spectrometry.

4.2. UPLC conditions

The analytical conditions for UPLC were set as follows. The mobile phase consisted of two components: Solvent A, which was ultrapure water with 0.04% acetic acid, and Solvent B, which was acetonitrile containing 0.04% acetic acid. A gradient elution strategy was adopted for sample analysis. At the beginning of the analysis, the mobile phase was 95% Solvent A and 5% Solvent B. Over a 10 - minute span, the proportion of Solvent A gradually decreased linearly to 5%, while that of Solvent B increased to 95%. This composition was then maintained for 1 minute. Subsequently, within 0.10 minutes, the mobile phase was swiftly reconfigured to 95% Solvent A and 5% Solvent B and kept at this ratio for 2.9 minutes. The column oven temperature was fixed at 40°C, and the injection volume was set at 2 μL. The effluent from the column was directly connected to an electrospray - triple quadrupole - linear ion trap (Q TRAP) mass spectrometer for further analysis.

4.3. ESI-Q TRAP-MS/MS

Analyses employed an API 6500 Q TRAP UPLC/MS/MS system with ESI Turbo Ion-Spray interface operating in dual polarity mode. To ensure precise measurements, the instrument was tuned and calibrated. In QQQ mode, a 10 μmol/L polypropylene glycol solution was used, while a 100 μmol/L polypropylene glycol solution was employed for calibration in linear ion trap mode.

During the QQQ scan, nitrogen was used as the collision gas at a pressure of 5 pounds per square inch for the multiple reaction monitoring (MRM) experiment. Each MRM transition was optimized based on the declustering potential and collision energy. These parameters were further refined to enhance the accuracy of metabolite detection. Based on

the eluted metabolites, a customized set of MRM transitions was monitored for each time period, enabling targeted and accurate analysis of the sample components.

4.4. Network pharmacological analysis

The chemical components of BKF were identified through the PubChem database . The pharmacokinetic characteristics of ABK were assessed with Swiss ADME. The pkCSM was used for toxicity evaluation. The targets of ABK on humans were obtained from databases such as Traditional Chinese Medicine Systems Pharmacology (TCMSP) , PharmMapper , ChemMapper, and Swiss Target prediction . Human-related targets of AS were collected using DisGeNET, OMIM, and GeneCards databases. Subsequently, DAVID bioinformatics resources were utilized to perform GO functional enrichment analysis and KEGG pathway analysis on the interaction targets. MEDWARE Data Bank and ChemDraw Professional 16.0 were used to draw 2D structures of 105 components of BKF. Cytoscape 3.6.1 was utilized for visualizing the network of drug-disease interaction targets.

4.5. Preparation of ABK

The fresh BKF was dried, crushed, and sieved through a 40-mesh sieve. Fat-soluble alkaloids (FSA) and water-soluble alkaloids (WSA) were prepared from 500 g of dried BKF powder using traditional extraction methods [72]. Both extracts were dried using a vacuum freeze-dryer. Total alkaloids (TA) were obtained from a mixture of FSA and WSA in a 1:1 ratio.

4.6. Cell line and treatment

RAW264.7 mouse macrophages, sourced from the Laboratory of Cell and Molecular Biology at the First Affiliated Hospital of Xinjiang Medical University, were cultured in high - glucose complete medium supplemented with 5% fetal bovine serum under standard conditions (37°C, 5% CO_2). For the treatment phase, the cells were subjected to different interventions. LPS (1 μg/mL; Solarbio, Beijing, China), FSA (at concentrations of 5, 10, and 25 μg/mL), WSA (25, 50, and 100 μg/mL), TA (10, 25, and 50 μg/mL), and OBB (5, 10, and 25 μg/mL; CAS: 549 - 21 - 3, HPLC purity 98%, Solarbio) were used. These substances were first dissolved in dimethyl sulfoxide (DMSO) and then diluted with PBS to ensure the final DMSO concentration was below 0.1%. The cells were exposed to these treatments for 24 hours. In contrast, the control group remained untreated.

4.7. ELISA

The expression levels of IL - 1β, IL - 18, MMP3, MMP9, and Caspase - 11 in the cell supernatant were quantified via ELISA. We utilized Mouse IL - 1β, IL - 18, MMP3, MMP9, and Caspase - 11 ELISA kits from Elabscience (Wuhan, China), strictly following the manufacturer's protocol. After the procedure, the optical density (OD) was measured at 450 nm.

4.8. Western blot analysis

Proteins were resolved on 12% SDS-PAGE gels (Bio-Rad) and transferred to PVDF membranes. After blocking (5% BSA/TBST), membranes were probed overnight at 4°C with primary antibodies: anti-GSDMD (#20770-1-AP, Proteintech), anti-pSTAT3 (#60479-1-lg, Proteintech), antianti-TLR4 (#19811-1-AP, Proteintech), and anti-β-actin (1:5,000, Sigma A5441). HRP-conjugated secondaries (1:10,000) were detected by ECL.

4.9. Caspase-1 activity analysis

The lysis solution was added after the interventions. The disrupted cells were centrifuged. Following the manufacturer's instructions for the mouse Caspase-1 activity detection kit (Solarbio), working reagents were sequentially added to each well, and the OD was measured at 450 nm.

4.10. Statistical methods

Data are expressed as mean ± SEM. Analyses were performed in GraphPad Prism 9.0 using: One-way ANOVA with Newman-Keuls post-hoc test for single-factor comparisons. Statistical significance was defined as $p < 0.05$ (*$p < 0.05$, **$p < 0.01$).

5. Conclusions

The UPLC-MS/MS analysis of BKF detected 544 metabolites, with 105 identified as secondary metabolites including flavonoids, polyphenols, alkaloids, sugars, saponins, coumarins, lignin, organic acids, and other components, indicating the rich medicinal and development potential of BKF. Of the 105 secondary metabolites, 24 were alkaloids. Analysis of the absorption, distribution, metabolism, and excretion process using TCMSP found that ABK had significant medicinal value. Moreover, 366 targets were predicted as anti-AS targets. The GO function enrichment analysis of these targets predicted that ABK may be involved in regulating lipid metabolism disorder, anti-inflammatory responses, antibacterial activity, apoptosis regulation, focal death, necrosis, and other programmed cell death, as well as participating in angiogenesis to fulfill its anti-AS role, providing a promising starting point for further research. KEGG and GO function enrichment analysis of the FSA and WSA groups predicted that the pharmacological action of FSA in BKF was biased towards lipid regulation, whereas the pharmacological action of WSA was biased towards antibacterial and anti-external stimulation, with both showing an anti-inflammatory effect. FSA, WSA, TA, and OBB significantly reduced the extracellular secretion of Caspase-11, IL-18, and IL-1β, as well as the expression of GSDMD-N protein in mouse macrophages stimulated by LPS. Furthermore, they decreased the intracellular Caspase-1 activity, inhibiting the non-classical pathway cell death caused by LPS. While different alkaloids in BKF exhibited distinct roles, many detailed issues persist, requiring further research and exploration. This study offers a specific experimental foundation for the future development and application of the therapeutic potential of BKA.

Supplementary Materials: Table S1: Compounds identified from BKF by UPLC-MS/MS.

Author Contributions: Conceptualization, S.A. and D.D.; methodology, S.A.; software, D.D; validation, S.A.; formal analysis, S.A. and D.D.; investigation, W.Z. and A.W.; data curation, S.A.; writing—original draft preparation, S.A.; writing—review and editing, W.Z. and A.W.; visualization, W.Z.; supervision, W.Z. and A.W.; project administration, W.Z.; funding acquisition, W.Z.. All authors have read and agreed to the published version of the manuscript. Figure 12 in the manuscript was drawn in Figdraw.

Funding: The authors appreciate financial support from the funding of the Tianshan Talents-Youth Science and Technology Innovation Talents Training Program of Xinjiang Autonomous Region (2022TSYCCX0035); Natural Science Foundation for Distinguished Young Scholars of Xinjiang Autonomous Region (2025); "Fourteenth Five-Year Plan" Key Discipline Construction Project of Xinjiang Autonomous Region (2021); Xinjiang Key Laboratory of Natural Medicines Active Components and Drug Release Technology (XJDX1713); Xinjiang Key Laboratory of Biopharmaceuticals and Medical Devices (2023); Engineering Research Center of Xinjiang and Central Asian Medicine Resources, Ministry of Education (2023).

Institutional Review Board Statement: Not applicable

Informed Consent Statement: Not applicable

Data Availability Statement: The datasets used and/or analysed during the current study are available from the corresponding author on reasonable request.

Acknowledgments: Not applicable

Conflicts of Interest: The authors declare no conflicts of interest. The funders had no role in the design of the study; in the collection, analyses, or interpretation of data; in the writing of the manuscript; or in the decision to publish the results.

Abbreviations

The following abbreviations are used in this manuscript:

BKF	*Berberis kaschgarica Rupr.* fruits	BKF
FSA	Fat-soluble alkaloids	FSA
OBB	Oxyberberine	OBB
TA	Total alkaloids	TA
WSA	Water-soluble alkaloids	WSA

References

1. Liao, C.P.; Liu, X.C.; Dong, S.Q.; An, M.; Zhao, L.; Zhang, A.J.; Liu, J.F.; Hou, W.B.; Fan, H.R.; Liu, C.X. Investigation of the metabolites of five major constituents from Berberis amurensis in normal and pseudo germ-free rats. *Chin J Nat Med* **2021**, *19*, 758-771, doi:10.1016/s1875-5364(21)60082-1.
2. Feng, T.; Xiao, Q.Y.; Li, W.J.; Zhang, C.; He, Y.; Fan, G. The complete chloroplast genome of Berberis weiningensis (Berberidaceae), an endemic and traditional Chinese medicinal herb. *Mitochondrial DNA B Resour* **2021**, *6*, 1175-1177, doi:10.1080/23802359.2021.1901625.
3. Wang, Y. Study on Chemical Constituents of Berries (Berberis kaschgarica Rupr.). *Journal of Tarim University* **2009**, *21*, 19-22.
4. Zhao, J.; Yang, L. Preliminary identification of anthocyanins in Berberis fruits in Xinjiang. *China Food Additives* **2011**, 121-124.
5. Sun, Y. Quality control of Berberis nigricans and application of near infrared spectroscopy in quality control. Xinjiang Medical University, Xinjiang, 2013.
6. Huang, J. Study on Antioxidant Characteristic of Anthocyanidin from Microencapsulated Berberis kaschgarica Rupr. *Journal of An Hui Agricultural Science* **2011**, *39*, 3244-3246.
7. Maierdan, Y.; Zhou, W.; Adilijiang, S.; Avaguli, D.; Jimirihan, S.; Adili, A.; Adila, D.; Ainivar, W. Relaxation effects of Berberis Kaschgarica Rupr. Fruit Water Extract on Isolated Thoracic Aortic Rings of Rats. *Chinese Traditional Patent Medicine* **2019**, *41*, 448-450, doi:10.3969/j.issn.1001-1528.2019.02.041.
8. Gui, T.; Shimokado, A.; Sun, Y.; Akasaka, T.; Muragaki, Y. Diverse roles of macrophages in atherosclerosis: from inflammatory biology to biomarker discovery. *Mediators Inflamm* **2012**, *2012*, 693083, doi:10.1155/2012/693083.
9. Bobryshev, Y.V.; Ivanova, E.A.; Chistiakov, D.A.; Nikiforov, N.G.; Orekhov, A.N. Macrophages and Their Role in Atherosclerosis: Pathophysiology and Transcriptome Analysis. *Biomed Res Int* **2016**, *2016*, 9582430, doi:10.1155/2016/9582430.
10. Tajbakhsh, A.; Rezaee, M.; Kovanen, P.T.; Sahebkar, A. Efferocytosis in atherosclerotic lesions: Malfunctioning regulatory pathways and control mechanisms. *Pharmacol Ther* **2018**, *188*, 12-25, doi:10.1016/j.pharmthera.2018.02.003.
11. Su, G.; Guan, X. Effects of macrophage apoptosis, pyroptosis and ferroptosis on the progression of atherosclerotic plaque. *International Journal of Immunology* **2020**, *43*, 336-341, doi:10.3760/cma.j.issn.1673-4394.2020.03.018.
12. Li, M.H.; Zhang, Y.J.; Yu, Y.H.; Yang, S.H.; Iqbal, J.; Mi, Q.Y.; Li, B.; Wang, Z.M.; Mao, W.X.; Xie, H.G., et al. Berberine improves pressure overload-induced cardiac hypertrophy and dysfunction through enhanced autophagy. *Eur J Pharmacol* **2014**, *728*, 67-76, doi:10.1016/j.ejphar.2014.01.061.
13. Zhao, G.L.; Yu, L.M.; Gao, W.L.; Duan, W.X.; Jiang, B.; Liu, X.D.; Zhang, B.; Liu, Z.H.; Zhai, M.E.; Jin, Z.X., et al. Berberine protects rat heart from ischemia/reperfusion injury via activating JAK2/STAT3 signaling and attenuating endoplasmic reticulum stress. *Acta Pharmacol Sin* **2016**, *37*, 354-367, doi:10.1038/aps.2015.136.
14. Miao, M.; Han, Y. Research progress of pyroptosis in coronary atherosclerosis. *International Journal of Cardiovascular Disease* **2023**, *50*, 144-147.

15. Gu, Y.; Tang, Z.; Wu, Y. The different roles of Inflammasomes/caspases pathway obout pyroptosis and cell apoptosis in atherosclerosis. *China Journal of Traditional Chinese Medicine* **2022**, *28*, 1378-1382.
16. Zhao, Z.; Ma, Y. Predictive effect of pyroptosis-related factors expression on atherosclerotic cardiovascular disease in patients with type 2 diabetes. *Chinese journal of health laboratory technology* **2023**, *33*, 323-326,331.
17. Zeng, X.; Guo, R.; Dong, M.; Zheng, J.; Lin, H.; Lu, H. Contribution of TLR4 signaling in intermittent hypoxia-mediated atherosclerosis progression. *J Transl Med* **2018**, *16*, 106, doi:10.1186/s12967-018-1479-6.
18. Gwon, W.G.; Joung, E.J.; Kwon, M.S.; Lim, S.J.; Utsuki, T.; Kim, H.R. Sargachromenol protects against vascular inflammation by preventing TNF-alpha-induced monocyte adhesion to primary endothelial cells via inhibition of NF-kappaB activation. *Int Immunopharmacol* **2017**, *42*, 81-89, doi:10.1016/j.intimp.2016.11.014.
19. Hiller, J.; Hagl, B.; Effner, R.; Puel, A.; Schaller, M.; Mascher, B.; Eyerich, S.; Eyerich, K.; Jansson, A.F.; Ring, J., et al. STAT1 Gain-of-Function and Dominant Negative STAT3 Mutations Impair IL-17 and IL-22 Immunity Associated with CMC. *J Invest Dermatol* **2018**, *138*, 711-714, doi:10.1016/j.jid.2017.09.035.
20. Li, Y.; Zhong, X.; Cheng, G.; Zhao, C.; Zhang, L.; Hong, Y.; Wan, Q.; He, R.; Wang, Z. Hs-CRP and all-cause, cardiovascular, and cancer mortality risk: A meta-analysis. *Atherosclerosis* **2017**, *259*, 75-82, doi:10.1016/j.atherosclerosis.2017.02.003.
21. Peterson, J.T.; Li, H.; Dillon, L.; Bryant, J.W. Evolution of matrix metalloprotease and tissue inhibitor expression during heart failure progression in the infarcted rat. *Cardiovasc Res* **2000**, *46*, 307-315, doi:10.1016/s0008-6363(00)00029-8.
22. Konstantino, Y.; Nguyen, T.T.; Wolk, R.; Aiello, R.J.; Terra, S.G.; Fryburg, D.A. Potential implications of matrix metalloproteinase-9 in assessment and treatment of coronary artery disease. *Biomarkers* **2009**, *14*, 118-129, doi:10.1080/13547500902765140.
23. Rasic, S.; Rebic, D.; Hasic, S.; Rasic, I.; Delic Sarac, M. Influence of Malondialdehyde and Matrix Metalloproteinase-9 on Progression of Carotid Atherosclerosis in Chronic Renal Disease with Cardiometabolic Syndrome. *Mediators Inflamm* **2015**, *2015*, 614357, doi:10.1155/2015/614357.
24. Kanehisa, M. et al. KEGG: biological systems database as a model of the real world. NucleicAcids Res. 53, D672–D677; 10.1093/nar/gkae909 (2025).
25. Kanehisa, M. & Goto, S. KEGG: Kyoto Encyclopedia of Genes and Genomes. Nucleic AcidsRes. 28, 27–30; http://www.genome.ad.jp/kegg/ (2000).
26. Kanehisa, M. Toward understanding the origin and evolution of cellular organisms. ProteinSci. 28, 1947–1951; 10.1002/pro.3715 (2019)。
27. Shi, X.; Xu, S. Research progress of pyroptosis and diseases related to human beings and animals *Journal of Tarim University* **2023**, *35*, 1-11.
28. Wang, B.; Wang, T.; Zhang, L.; Zhang, S.; Zhang, D. Research progress of inflammatory corpuscles and pyroptosis in intestinal homeostasis. *China Journal of Immunology* **2023**, *39*, 1337-1341.
29. Wu, D.; Yang, J.; Zhang, C. Application progress of LC-MS in Polygonaceae Chinese medicinal materials. *China Pharmacy* **2014**, *25*, 2179-2181, doi:CNKI:SUN:ZGYA.0.2014-23-027.
30. Alifeire, A.; Adili, A.; Imranjiang, S.; Abulaiti, A.; Zhou, W.; Ainiwal, W. Effects of Berberis Kashi extract on blood lipid and inflammation-related indexes in atherosclerotic rats. *Zhongnan Pharmacy* **2022**, *20*, 1052-1056.
31. Sinning, D.; Leistner, D.M.; Landmesser, U. [Impact of lipid metabolism parameters on the development and progression of coronary artery disease : An update]. *Herz* **2016**, *41*, 273-280, doi:10.1007/s00059-016-4430-8.
32. Zhang, H.; Ren, B.; Ji, Y.; Gu, J.; Zheng, Z.; Liu, W. Programmed death of macrophages in atherosclerosis. *China journal of modern medicine* **2023**, *33*, 43-49.
33. Xiao, F.; Gong, L.; Zhao, S. Discussion on the correlation between atherosclerosis and mitochondrial autophagy based on the theory of phlegm and blood stasis generating wind. *Chinese Medicine Herald* **2023**, *29*, 105-107,116.
34. Wang, J. Research progress on the relationship between mitochondrial dynamics/autophagy and the stability of atherosclerotic plaques. *Modern Medicine and Health* **2022**, *38*, 3318-3321,3325.

35. He, L.; Zhou, Q.; Huang, Z.; Xu, J.; Zhou, H.; Lv, D.; Lu, L.; Huang, S.; Tang, M.; Zhong, J., et al. PINK1/Parkin-mediated mitophagy promotes apelin-13-induced vascular smooth muscle cell proliferation by AMPKalpha and exacerbates atherosclerotic lesions. *J Cell Physiol* **2019**, *234*, 8668-8682, doi:10.1002/jcp.27527.
36. Peng, X.; Chen, H.; Li, Y.; Huang, D.; Huang, B.; Sun, D. Effects of NIX-mediated mitophagy on ox-LDL-induced macrophage pyroptosis in atherosclerosis. *Cell Biol Int* **2020**, *44*, 1481-1490, doi:10.1002/cbin.11343.
37. Li, C.; Ai, G.; Wang, Y.; Lu, Q.; Luo, C.; Tan, L.; Lin, G.; Liu, Y.; Li, Y.; Zeng, H., et al. Oxyberberine, a novel gut microbiota-mediated metabolite of berberine, possesses superior anti-colitis effect: Impact on intestinal epithelial barrier, gut microbiota profile and TLR4-MyD88-NF-kappaB pathway. *Pharmacol Res* **2020**, *152*, 104603, doi:10.1016/j.phrs.2019.104603.
38. Zhao, R.; Wang, B.; Wang, D.; Wu, B.; Ji, P.; Tan, D. Oxyberberine Prevented Lipopolysaccharide-Induced Acute Lung Injury through Inhibition of Mitophagy. *Oxid Med Cell Longev* **2021**, *2021*, 6675264, doi:10.1155/2021/6675264.
39. Dou, Y.; Huang, R.; Li, Q.; Liu, Y.; Li, Y.; Chen, H.; Ai, G.; Xie, J.; Zeng, H.; Chen, J., et al. Oxyberberine, an absorbed metabolite of berberine, possess superior hypoglycemic effect via regulating the PI3K/Akt and Nrf2 signaling pathways. *Biomed Pharmacother* **2021**, *137*, 111312, doi:10.1016/j.biopha.2021.111312.
40. Anwar, M.A.; Tabassam, S.; Gulfraz, M.; Sheeraz Ahmad, M.; Raja, G.K.; Arshad, M. Isolation of Oxyberberine and β-Sitosterol from Berberis lycium Royle Root Bark Extract and In Vitro Cytotoxicity against Liver and Lung Cancer Cell Lines. *Evid Based Complement Alternat Med* **2020**, *2020*, 2596082, doi:10.1155/2020/2596082.
41. Yuan, Y.; Dong, F.X.; Liu, X.; Xiao, H.B.; Zhou, Z.G. Liquid Chromatograph-Mass Spectrometry-Based Non-targeted Metabolomics Discovery of Potential Endogenous Biomarkers Associated With Prostatitis Rats to Reveal the Effects of Magnoflorine. *Front Pharmacol* **2021**, *12*, 741378, doi:10.3389/fphar.2021.741378.
42. Zhao, F.; Guo, Z.; Hou, F.; Fan, W.; Wu, B.; Qian, Z. Magnoflorine Alleviates "M1" Polarized Macrophage-Induced Intervertebral Disc Degeneration Through Repressing the HMGB1/Myd88/NF-κB Pathway and NLRP3 Inflammasome. *Front Pharmacol* **2021**, *12*, 701087, doi:10.3389/fphar.2021.701087.
43. Sun, Z.; Zeng, J.; Wang, W.; Jia, X.; Wu, Q.; Yu, D.; Mao, Y. Magnoflorine Suppresses MAPK and NF-κB Signaling to Prevent Inflammatory Osteolysis Induced by Titanium Particles In Vivo and Osteoclastogenesis via RANKL In Vitro. *Front Pharmacol* **2020**, *11*, 389, doi:10.3389/fphar.2020.00389.
44. Liu, Y.T.; Hao, H.P.; Xie, H.G.; Lai, L.; Wang, Q.; Liu, C.X.; Wang, G.J. Extensive intestinal first-pass elimination and predominant hepatic distribution of berberine explain its low plasma levels in rats. *Drug Metab Dispos* **2010**, *38*, 1779-1784, doi:10.1124/dmd.110.033936.
45. Zuo, F.; Nakamura, N.; Akao, T.; Hattori, M. Pharmacokinetics of berberine and its main metabolites in conventional and pseudo germ-free rats determined by liquid chromatography/ion trap mass spectrometry. *Drug Metab Dispos* **2006**, *34*, 2064-2072, doi:10.1124/dmd.106.011361.
46. Arumugam, M.K.; Paal, M.C.; Donohue, T.M., Jr.; Ganesan, M.; Osna, N.A.; Kharbanda, K.K. Beneficial Effects of Betaine: A Comprehensive Review. *Biology (Basel)* **2021**, *10*, doi:10.3390/biology10060456.
47. Hu, S.; Li, H.; Kang, P.; Chen, T.; Li, M.; Zhu, J.; Gao, D.; Zhang, H.; Wang, H. Simvastatin inhibits apoptosis by up-regulating the expression of Bcl-2 protein in vascular wall of atherosclerotic rats. *Journal of Southern Medical University* **2017**, *37*, 1456-1460, doi:10.3969/j.issn.1673-4254.2017.11.05.
48. Chen, Y.; Ding, H.; Li, G.; Wang, L. Effects of Ad-FLT-1/PC on apoptosis and oxidative stress in diabetic nephropathy atherosclerotic rats. *Chinese Journal of Nephrology* **2017**, *33*, 770-774, doi:10.3760/cma.j.issn.1001-7097.2017.10.008.
49. Wang, D.; Feng, R.; Shi, S.; Wei, N.; Hu, Y. Research progress of oxidative stress associated with CD36 in atherosclerosis. *Journal of Cardiovascular and Cerebrovascular Diseases of Integrated Traditional Chinese and Western Medicine* **2022**, *20*, 1015-1020.
50. Hou, Y.; Lin, F.; Li, Y.; Guan, S.; Meng, W.; Zhao, G. Research progress on the role of oxidative stress in the pathogenesis of atherosclerosis. *Journal of Xinxiang Medical College* **2021**, *38*, 1090-1094.
51. Zeng, Z.; Li, G.; Wu, S.; Wang, Z. Role of pyroptosis in cardiovascular disease. *Cell Prolif* **2019**, *52*, e12563, doi:10.1111/cpr.12563.

52. Xu, J.; Liu, F.; Liu, Y.; Song, S.; Liu, K.; Zhao, Q. Relationship between macrophage apoptosis and plaque vulnerability in atherosclerotic plaques. *Journal of College of Military Medical Training* **2008**, *29*, 289-291.
53. Liu, Y.; Sun, Y.; Yang, A.; Liu, Z.; Liu, T.; Hao, W.; Liu, Y.; Wang, Q.; Liu, Z. Iron death is involved in atherosclerosis induced by high-fat diet and foam cell formation induced by ox-LDL in ApoE-/- mice. *Journal of Practical Medicine* **2021**, *37*, 585-590, doi:10.3969/j.issn.1006-5725.2021.05.006.
54. Hoseini, Z.; Sepahvand, F.; Rashidi, B.; Sahebkar, A.; Masoudifar, A.; Mirzaei, H. NLRP3 inflammasome: Its regulation and involvement in atherosclerosis. *J Cell Physiol* **2018**, *233*, 2116-2132, doi:10.1002/jcp.25930.
55. Broz, P. Immunology: Caspase target drives pyroptosis. *Nature* **2015**, *526*, 642-643, doi:10.1038/nature15632.
56. Shi, J.; Zhao, Y.; Wang, K.; Shi, X.; Wang, Y.; Huang, H.; Zhuang, Y.; Cai, T.; Wang, F.; Shao, F. Cleavage of GSDMD by inflammatory caspases determines pyroptotic cell death. *Nature* **2015**, *526*, 660-665, doi:10.1038/nature15514.
57. Liu, X.; Zhang, Z.; Ruan, J.; Pan, Y.; Magupalli, V.G.; Wu, H.; Lieberman, J. Inflammasome-activated gasdermin D causes pyroptosis by forming membrane pores. *Nature* **2016**, *535*, 153-158, doi:10.1038/nature18629.
58. Ding, J.; Wang, K.; Liu, W.; She, Y.; Sun, Q.; Shi, J.; Sun, H.; Wang, D.C.; Shao, F. Pore-forming activity and structural autoinhibition of the gasdermin family. *Nature* **2016**, *535*, 111-116, doi:10.1038/nature18590.
59. Evavold, C.L.; Ruan, J.; Tan, Y.; Xia, S.; Wu, H.; Kagan, J.C. The Pore-Forming Protein Gasdermin D Regulates Interleukin-1 Secretion from Living Macrophages. *Immunity* **2018**, *48*, 35-44 e36, doi:10.1016/j.immuni.2017.11.013.
60. Wang, K.; Sun, Q.; Zhong, X.; Zeng, M.; Zeng, H.; Shi, X.; Li, Z.; Wang, Y.; Zhao, Q.; Shao, F., et al. Structural Mechanism for GSDMD Targeting by Autoprocessed Caspases in Pyroptosis. *Cell* **2020**, *180*, 941-955 e920, doi:10.1016/j.cell.2020.02.002.
61. Humphries, F.; Shmuel-Galia, L.; Ketelut-Carneiro, N.; Li, S.; Wang, B.; Nemmara, V.V.; Wilson, R.; Jiang, Z.; Khalighinejad, F.; Muneeruddin, K., et al. Succination inactivates gasdermin D and blocks pyroptosis. *Science* **2020**, *369*, 1633-1637, doi:10.1126/science.abb9818.
62. Barnett, K.C.; Ting, J.P. Mitochondrial GSDMD Pores DAMPen Pyroptosis. *Immunity* **2020**, *52*, 424-426, doi:10.1016/j.immuni.2020.02.012.
63. Virmani, R.; Kolodgie, F.D.; Burke, A.P.; Finn, A.V.; Gold, H.K.; Tulenko, T.N.; Wrenn, S.P.; Narula, J. Atherosclerotic plaque progression and vulnerability to rupture: angiogenesis as a source of intraplaque hemorrhage. *Arterioscler Thromb Vasc Biol* **2005**, *25*, 2054-2061, doi:10.1161/01.ATV.0000178991.71605.18.
64. Luttun, A.; Lutgens, E.; Manderveld, A.; Maris, K.; Collen, D.; Carmeliet, P.; Moons, L. Loss of matrix metalloproteinase-9 or matrix metalloproteinase-12 protects apolipoprotein E-deficient mice against atherosclerotic media destruction but differentially affects plaque growth. *Circulation* **2004**, *109*, 1408-1414, doi:10.1161/01.CIR.0000121728.14930.DE.
65. Ezzahiri, R.; Stassen, F.R.M.; Kurvers, H.R.M.; Dolmans, V.; Bruggeman, C.A. Chlamydia pneumoniae infections augment atherosclerotic lesion formation: a role for serum amyloid P. *APMIS* **2006**, *114*, 117-126, doi: 10.1111/j.1600-0463.2006.apm_205.x.
66. Do, G.M.; Kwon, E.Y.; Kim, H.J.; Jeon, S.M.; Ha, T.Y.; Park, T.; Choi, M.S. Long-term effects of resveratrol supplementation on suppression of atherogenic lesion formation and cholesterol synthesis in apo E-deficient mice. *Biochem Biophys Res Commun* **2008**, *374*, 55-59, doi:10.1016/j.bbrc.2008.06.113.
67. Chen, B. Study on the protective effect of berberine oxide on mice with acute lung injury. Guangzhou University of Chinese Medicine, Guangdong, 2021.
68. Hu, Y. Research progress on the transduction mechanism of mTOR and STAT3, the key signal pathways of resveratrol in the treatment of atherosclerosis. *Journal of Kunming Medical University* **2013**, *34*, 164-168.
69. Rahmani, S.; Nasiri, M.; Gholami, M.; et al. Berberis vulgaris Fruit Extract Improves Lipid Profile in Patients with Metabolic Syndrome: A Randomized, Double-Blind, Placebo-Controlled Trial. *J Ethnopharmacol* **2023**, *316*, 116872.
70. Zhang, Y.; Li, J.; Wang, H.; et al. Berberine Inhibits Atherosclerotic Plaque Progression by Suppressing Macrophage Foam Cell Formation via the ABCA1/APOA1 Pathway. *Int J Mol Sci* **2022**, *23*, 14890.
71. Singh, R.; Sharma, A.; Gupta, S.; et al. Alkaloids from Berberis aristata Mitigate LPS-Induced Inflammation via TLR4/NF-κB Pathway Inhibition. *Phytomedicine* **2023**, *112*, 154890.

72. Cui, J.; Chen, X.; Sun, Z.; Zhang, H. Extraction of alkaloids from Solanum lyratum Thunb. and its antibacterial activity in vitro. *Journal of traditional chinese veterinary medicine* **2004**, *2004*, 41-42, doi:10.3969/j.issn.1000-6354.2004.05.022.